AD-768 841

EXPERIMENTS IN MULTI-DIMENSIONAL FLOATING SHOCK-FITTING

Gino Moretti

Polytechnic Institute of Brooklyn

Prepared for:

Office of Naval Research

August 1973

DISTRIBUTED BY:

NTIS

National Technical Information Service
U. S. DEPARTMENT OF COMMERCE
5285 Port Royal Road, Springfield Va. 22151

Unclassified
Security Classification

AD-768 841

DOCUMENT CONTROL DATA - R & D

(Security classification of title, body of abstract and indexing annotation must be entered when the overall report is classified)

1 ORIGINATING ACTIVITY (Corporate author) Polytechnic Institute of Brooklyn Dept. of Aerospace Engrg. and Applied Mech. Route 110, Farmingdale, New York 11735	2a. REPORT SECURITY CLASSIFICATION Unclassified 2b. GROUP

3 REPORT TITLE
EXPERIMENTS IN MULTI-DIMENSIONAL FLOATING SHOCK-FITTING

4 DESCRIPTIVE NOTES (Type of report and inclusive dates)
Research report

5 AUTHOR(S) (First name, middle initial, last name)
GINO MORETTI

6 REPORT DATE	7a. TOTAL NO. OF PAGES	7b. NO. OF REFS
August 1973	~~38~~ 52	16

8a. CONTRACT OR GRANT NO. N00014-67-A-0438-0009 b. PROJECT NO. NR 061-135 c. d.	9a. ORIGINATOR'S REPORT NUMBER(S) PIBAL Report No. 73-18 9b. OTHER REPORT NO(S) (Any other numbers that may be assigned this report)

10 DISTRIBUTION STATEMENT
Approved for public release; distribution unlimited.

11 SUPPLEMENTARY NOTES	12 SPONSORING MILITARY ACTIVITY
	Office of Naval Research Code 438 Arlington, Virginia 22217

13 ABSTRACT

Four numerical experiments are performed to support floating shock-fitting techniques in multi-dimensional flow problems. By floating shock-fitting we mean the fitting of a shock as a sharp discontinuity, free of moving within the computational mesh. Evidences of accuracy and stability are given.

DD FORM 1 NOV 65 1473

Unclassified
Security Classification

Unclassified
Security Classification

14. KEY WORDS	LINK A		LINK B		LINK C	
	ROLE	WT	ROLE	WT	ROLE	WT
Compressible flow Numerical analysis Conical flow Floating shock-fitting						

Unclassified
Security Classification

EXPERIMENTS IN MULTI-DIMENSIONAL FLOATING SHOCK-FITTING

by

Gino Moretti

This research was conducted under the sponsorship of the Office of Naval Research under Contract No. N00014-67-A-0438-0009, Project No. NR 061-135.

POLYTECHNIC INSTITUTE OF BROOKLYN

Department

of

Aerospace Engineering and Applied Mechanics

August 1973

PIBAL Report No. 73-18

EXPERIMENTS IN MULTI-DIMENSIONAL FLOATING SHOCK-FITTING

by

Gino Moretti*

Polytechnic Institute of Brooklyn
Preston R. Bassett Research Laboratory
Farmingdale, New York

ABSTRACT

Four numerical experiments are performed to support floating shock-fitting techniques in multi-dimensional flow problems. By floating shock-fitting we mean the fitting of a shock as a sharp discontinuity, free of moving within the computational mesh. Evidences of accuracy and stability are given.

*Professor, Dept. of Aerospace Engineering and Applied Mechanics.

TABLE OF CONTENTS

I. INTRODUCTION

In the controversy between supporters of shock-fitting and shock-capturing techniques, I have tried to establish a few basic points in support of the shock-fitting approach

1) Shock-capturing is a poor interpretation of a physical phenomenon and is, to say the least, an extremely uneconomical way of computing.[1-5]

2) Prediction of imbedded shock formation in one-dimensional problems and in multi-dimensional problems as well is possible and simple, in the general framework of finite-difference techniques.[2-7]

3) Shock-fitting works not only if the shock is one of the boundaries of a single computational region[9-12] but also if the shock is a boundary between two computational regions, in one-dimensional problems[1,3-5] and in multi-dimensional problems as well.[6-8] The work reported in Ref. 8 has currently been extended to flow fields with additional cross-flow shocks; the yet unpublished results show the overwhelming superiority of shock-fitting to shock-capturing in a very complicated problem, and, as the authors of Ref. 8 point out, should exhaustily answer certain objections raised against shock-fitting in more than one dimension.

The case for shock-fitting techniques, however, is not completed without proving that shock-fitting is also feasible and accurate when shocks are not fitted as boundaries of computational regions. In multi-dimensional problems, indeed, we may have good reasons for fitting imbedded shocks without subdividing the computational region into partial regions bounded by them, at least in part; in other words, we may wish to let the shocks (treated as sharp discontinuities) float among mesh points. There is no advantage in so doing when the number of space-like dimensions is one; there are advantages instead in multi-dimensional problems with very complicated shock patterns, since the logic necessary to handle the topology of shock-bounded regions seems to be too complex and, anyhow, more complex than the logic of floating shocks. Questions, however, have been asked about the numerical stability of the approach,[16] and there is a good deal of skepticism on its practicality.[13]

In forthcoming papers, I intend to apply floating shock-fitting to practical problems of increasing difficulty:

a) Three-dimensional, steady, supersonic flows past simple, wingless airframes (such as in Ref. 8 but without wings, to eliminate lengthy mappings which are irrelevant to the present discussion),

b) Transonic (supercritical) flow past a boattail by a time-dependent technique (to be compared with the results of Ref. 6),

c) Transonic (supercritical) flow past a cylinder by a time-dependent technique (to complete the analysis of Ref. 15),

d) Steady, supersonic flow past cones at yaw, with formation of cross-flow shock (to complete the analysis of Ref. 12),

e) Three-dimensional nozzle flows with multiple shocks, etc.

As a preliminary work, I have studied one-dimensional, unsteady flows with shocks fitted among mesh points[4] in order to understand the numerical difficulties connected with the passing of the shock from one mesh interval to the next, and I have concluded that the techniques developed in Ref. 4 are safe, stable, and accurate. In the present report, I intend to present preliminary exercises on multi-dimensional problems, to pave the way for the applications mentioned above under a-e.

The reader should not anticipate anything spectacular in these exercises; they are kept in a low key on purpose, to make the analysis simple and to reveal the nature of the difficulties and the steps to take without unnecessary complications, irrelevant to the basic problem of floating shock fitting.

II. FOUR VARIATIONS ON THE SAME THEME

The first flow field we are going to examine is simply the classical supersonic flow, uniform at infinity, past a pointed cone (with a circular cross section) at no incidence. The flow is conical and axisymmetrical and we may get a very accurate picture of the shock layer by integrating an ordinary differential equation. Therefore, we have an "exact" solution of the problem, which we may use to test the accuracy of our computations.

We will pretend we ignore the axisymmetric, conical nature of the flow; we will start at a station, $z=0$, somewhere downstream from the apex of the cone, using the exact solution to provide initial values; for increasing values of z we will compute the flow using a three-dimensional, finite-difference technique with floating shock-fitting. To analyze the floating shock-fitting technique we need a computational region wider than the shock layer; therefore, we use an outer boundary arbitrarily located in the region of uniform flow. A proper choice of the shape of the outer boundary (a cone with the same apex and the same axis as the body) keeps the frame of reference axisymmetrical, and the problem in this case depends on one space-like dimension only. A cross-section of the flow field will appear as in Fig. 1a;

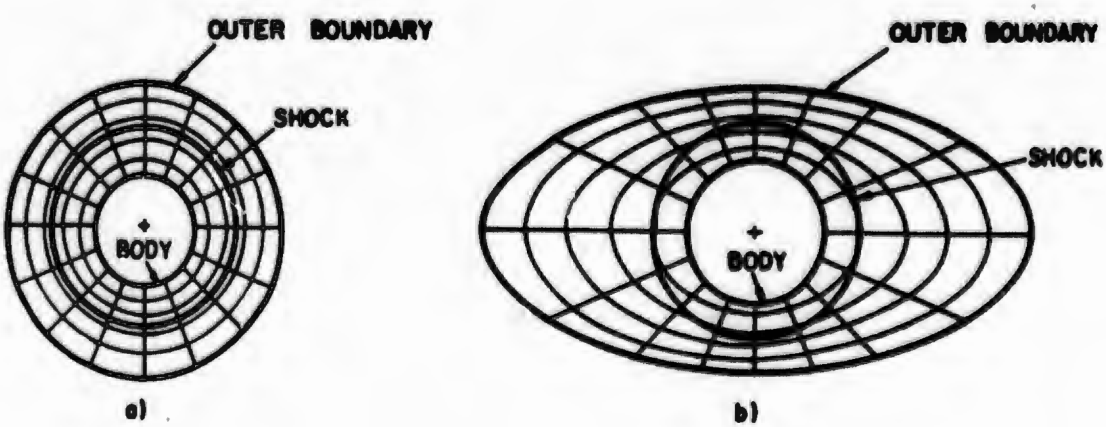

Fig. 1

no peripheral effects will appear; the shock will float among mesh points only radially.

If the shape of the outer boundary is chosen differently (for example, as in Fig. 1b, with elliptical cross-sections) and the radial coordinate is normalized between the body and the outer boundary, three-dimensional effects will be introduced into the computation of a flow which is physically axisymmetrical. For example, the (conical) floating shock will have to cross mesh lines in both directions. When expressed in cylindrical coordinates, however, the solution should be identical with the exact solution.

In the third and fourth problems to be considered in this report, the body itself has an elliptic cross-section. The eccentricity of the ellipse is 0 at z=0 and varies with z; the flow, thus, is the same as in the previous cases at z=0 and then becomes really three-dimensional. Two cases again may be considered, according to the geometry of the outer boundary (Fig. 2).

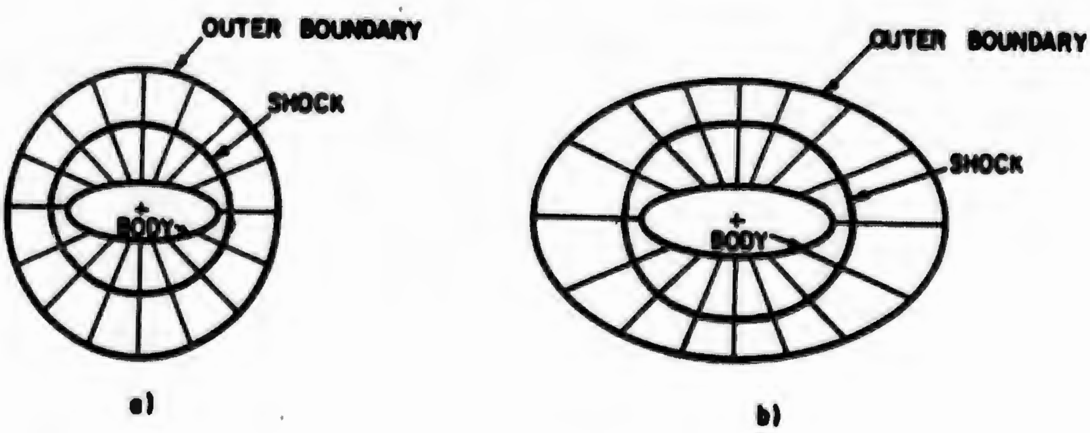

Fig. 2

III. FRAME OF REFERENCE AND BASIC EQUATIONS OF MOTION

The basic frame of reference for all four cases is a cylindrical frame, whose z-axis lies along the axis of the body; r and θ are, as usual, the radial coordinate and the angle between a fixed meridional plane and any other meridional plane. The body is defined by

(1) $$r=b(z)=b_1+z\tan\delta \qquad \text{(case 1, case 2)}$$

where b_1 is the radius of the cross-section of the cone at z=0 and δ is the semiaperture of the cone; or by

(2) $$r=b(\theta,z)=\left[\frac{\cos^2\theta}{A_o^2(z)}+\frac{\sin^2\theta}{B_o^2(z)}\right]^{-\frac{1}{2}} \qquad \text{(case 3, case 4)}$$

where

(3) $$\begin{cases} A_o = b_1+z\tan\delta \\ B_o = \begin{cases} b_1+z\tan\delta+b_2z^2+b_3z^3 & (0\le z\le z_o) \\ b_o & (z>z_o) \end{cases} \end{cases}$$

and b_2 and b_3 are such that $B_o(z_o)=b_o$, $B_o'(z_o)=0$.

The outer boundary is defined by

(4) $$r=c(z)=c_1+z\tau\tan\delta \qquad \text{(case 1, case 3)}$$

where c_1 is the radius of the cross-section of the outer boundary at z=0 and τ is an arbitrary parameter; or by

(5) $$r=c(\theta,z)=\left[\frac{\cos^2\theta}{A^2(z)}+\frac{\sin^2\theta}{B^2(z)}\right]^{-\frac{1}{2}} \qquad \text{(case 2, case 4)}$$

where

(6) $$\begin{cases} A(z)=c_1+z\sigma\tan\delta \\ B(z)=c_1+z\tau\tan\delta \end{cases}$$

Again, σ and τ will be arbitrary parameters. At z=0, $c(\theta,0)=c_1$ as in cases 1 and 3.

Several derivatives of b and c are necessary in our calculations; they are easily obtained and reported here:

(7) $$b_z = \tan\delta,\ b_\theta = 0,\ b_{\theta z} = 0,\ b_{zz} = 0 \qquad \text{(case 1, case 2)}$$

$$b_z = -b^3\left[\frac{\cos^2\theta}{A_o^3} A_{oz} + \frac{\sin^2\theta}{B_o^3} B_{oz}\right] \qquad \text{(case 3, case 4)}$$

(8) $$b_\theta = b^3\left[\frac{1}{A^3_o} - \frac{1}{B^3_o}\right]\sin\theta\cos\theta$$

$$b_{\theta z} = b^3 \left[3b_z\left(\frac{1}{A_o^3} - \frac{1}{B_o^3}\right) - 2b\left(\frac{A_{oz}}{A_o^3} - \frac{B_{oz}}{B_o^3}\right)\right]\sin\theta\cos\theta$$

$$b_{zz} = -3b^2 b_z\left(\frac{\cos^2\theta}{A_o^3} A_{oz} + \frac{\sin^2\theta}{B_o^3} B_{oz}\right) -$$

$$-b^3\left[\cos^2\theta \left(\frac{A_{ozz}}{A_o^3} - \frac{3A_{oz}^2}{A_o^4}\right) + \sin^2\theta \left(\frac{B_{ozz}}{B_o^3} - \frac{3B_{oz}^2}{B_o^4}\right)\right]$$

where

(9) $$A_{oz} = \tan\delta \qquad A_{ozz} = 0$$

(10) $$B_{oz} = \begin{cases} \tan\lambda + 2b_2 z + 3b_3 z^2 \\ 0 \end{cases} \qquad B_{ozz} = \begin{cases} 2b+6b_3 z & (0 \le z \le z_o) \\ 0 & (z > z_o) \end{cases}$$

(11) $$c_z = \tau\tan\delta\ ,\ c_\theta = 0\ ,\ c_{\theta z} = 0\ ,\ c_{zz} = 0 \qquad \text{(Case 1, Case 3)}$$

$$\begin{cases} c_z = -c^3\left[\frac{\cos^2\theta}{A^3} A_z + \frac{\sin^2\theta}{B^3} B_z\right] \qquad \text{(Case 2, Case 4)} \\ c_\theta = c\ \left[\frac{1}{A^3} - \frac{1}{B^3}\right]\sin\theta\cos\theta \\ c_{\theta z} = c^3\left[3c_z\left(\frac{1}{A^3} - \frac{1}{B^3}\right) - 2c\left(\frac{A_z}{A^3} - \frac{B_z}{B^3}\right)\right]\sin\theta\cos\theta \\ c_{zz} = -3c^2 c_z\left(\frac{\cos^2\theta}{A^3} A_z + \frac{\sin^2\theta}{B^3} B_z\right) - c^3\left[\cos^2\theta\left(\frac{A_{zz}}{A^3} - \frac{3A_z^2}{A^4}\right) + \right. \\ \left. + \sin^2\theta\left(\frac{B_{zz}}{B^3} - \frac{3B_z^2}{B^4}\right)\right] \end{cases}$$

where

(13) $$A_z = \sigma\tan\delta\ ,\ B_z = \tau\tan\delta\ ,\ A_{zz} = B_{zz} = 0$$

The frame of reference will be normalized by the transformation

(14) $$X = \frac{r-b}{c-b} \quad , \quad Y=\theta \quad , \quad Z=z$$

which yields

(15) $$X_r = \frac{1}{c-b} \quad , \quad X_\theta = X_r[(X-1)b_\theta - Xc_\theta] \quad , \quad X_z = X_r[(X-1)b_z - Xc_z]$$

(16) $$Y_r=0 \quad , \quad Y_\theta=1 \quad , \quad Y_z=0$$

(17) $$Z_r=0 \quad , \quad Z_\theta=0 \quad , \quad Z_z=1$$

Consequently, for any function $f(r,\theta,z)$,

(18) $$\begin{cases} f_r = f_X X_r \\ f_\theta = f_Y + f_X X_\theta \\ f_z = f_Z + f_X X_z \end{cases}$$

The equations of motion in the physical space, in cylindrical coordinates, are

$$\begin{cases} uP_r + \frac{v}{r} P_\theta + wP_z + \gamma(u_r + \frac{1}{r} v_\theta + w_z + \frac{u}{r}) = 0 \\ uu_r + \frac{v}{r} u_\theta + wu_z + \mathcal{J} P_r - \frac{v^2}{r} = 0 \\ uv_r + \frac{v}{r} v_\theta + wv_z + \frac{\mathcal{J}}{r} P_\theta + \frac{uv}{r} = 0 \\ uw_r + \frac{v}{r} w_\theta + ww_z + \mathcal{J} P_z = 0 \\ uS_r + \frac{v}{r} S_\theta + wS_z = 0 \end{cases}$$

where

(20) $$P = \ln p/p_\infty$$

(21) $$\mathcal{J} = \frac{p/p_\infty}{\rho/\rho_\infty}$$

(22) $$S = \ln p/p_\infty - \gamma \ln \rho/\rho_\infty$$

and the cylindrical velocity components, u,v, and w, are expressed as multiples of

$$u_{ref} = \sqrt{p_\infty / \rho_\infty} \qquad (23)$$

With the above assumptions, the problem is defined once the cone semi-angle, δ, the Mach number at infinity, M_∞ and the ratio of specific heats, γ, are assigned. In particular, the velocity at infinity is

$$V_\infty = \sqrt{\gamma}\, M_\infty \qquad (24)$$

In the (X,Y,Z) frame of reference and in matrix form, (19) become

$$f_Z = \mathbf{A} f_X + \mathbf{B} f_Y + \mathbf{C} \qquad (25)$$

where

$$(26)\quad \begin{cases} f = \begin{bmatrix} p \\ u \\ v \\ w \\ S \end{bmatrix}, \quad \mathbf{A} = \begin{bmatrix} (a^2 X_z - \Lambda w)\Delta & -\gamma \Delta w X_r & -\gamma \Delta w X_\theta / r & \gamma \Delta (\Lambda - w X_z) & 0 \\ -\mathcal{J} X_r / w & -\Lambda / w & 0 & 0 & 0 \\ -\mathcal{J} X_\theta / rw & 0 & -\Lambda / w & 0 & 0 \\ \mathcal{J} \Delta (\Lambda - w X_z) & a^2 \Delta X_r & a^2 \Delta X_\theta / r & (a^2 X_z - w\Lambda)\Delta & 0 \\ 0 & 0 & 0 & 0 & -\Lambda / w \end{bmatrix} \\ \mathbf{B} = \begin{bmatrix} -vw\Delta/r & 0 & -\gamma \Delta w / r & \gamma \Delta v / r & 0 \\ 0 & -v/rw & 0 & 0 & 0 \\ -\mathcal{J}/rw & 0 & -v/rw & 0 & 0 \\ \mathcal{J} \Delta v / r & 0 & a^2 \Delta / r & -\Delta w v / r & 0 \\ 0 & 0 & 0 & 0 & -v/rw \end{bmatrix}, \quad \mathbf{C} = \begin{bmatrix} -\gamma u w \Delta / r \\ v^2 / rw \\ -uv/rw \\ a^2 \Delta u / r \\ 0 \end{bmatrix} \end{cases}$$

with

$$\Lambda = u X_r + \frac{v}{r} X_\theta + w X_z \, , \quad \Delta = 1/(w^2 - a^2) \, , \quad a = \sqrt{\gamma \mathcal{J}} \qquad (27)$$

IV. A CHARACTERISTIC EQUATION

To treat the shock, we need a compatibility equation along a characteristic lying on the (ξ, ζ) plane of a frame of reference defined as follows:

(28)
$$\xi = \frac{r-b}{s-b}$$
$$\eta = \theta$$
$$\zeta = z$$

where

(29)
$$r = s\ (\theta, z)$$

is the shock surface. To treat the boundary conditions on the body we also need a compatibility equation along a characteristic lying on the (X,Y) plane. Here I will obtain both characteristics using the symbols defined by (28). Note that $\xi=0$, as well as X=0, represents the body surface, whereas $\xi=1$ represents the shock surface. Therefore, derivatives with respect to η at $\xi=0$ coincide with derivatives with respect to Y at X=0 and are θ-derivatives taken along the cross-section of the body at a constant z, whereas derivatives with respect to η at $\xi=1$ are θ-derivatives taken along the cross-section of the shock at a constant z. Similarly, derivatives with respect to ζ at $\xi=0$ coincide with derivatives with respect to Z at X=0 and are z-derivatives taken along the section of the body with a meridional plane, whereas derivatives with respect to ζ at $\xi=1$ are z-derivatives taken along the section of the shock with a meridional plane. The derivatives with respect to ξ, instead, differ from the derivatives with respect to X because of the different scaling.

The system of equations from which we extract the characteristic equation is similar to (25), (26), (27), with X,Y,Z replaced by ξ, η, ζ respectively. From the first, second, and fourth of such equations, we obtain a linear combination,

$$\mu_1(P_\zeta+\lambda P_\xi) + \mu_2(u_\zeta+\lambda u_\xi) + \mu_3(w_\zeta+\lambda w_\xi) + \mu_1 R_1+\mu_2 R_2+\mu_3 R_3 = 0 \tag{30}$$

where

$$\left\{\begin{aligned} & B=u\xi_r+\frac{v}{r}\xi_\theta \;,\; \mu_1=\pm a\sqrt{\xi_r^2/\Delta+B^2} \;,\; \mu_2=-\gamma w\xi_r \;,\; \mu_3=\gamma B \\ & \lambda = \xi_z+w\Delta B-\mu_1\Delta \\ & R_1 = \frac{\Delta}{r}\left[vwP_\eta+\gamma w(v_\xi\xi_\theta+v_\eta+u)-vw w_\eta\right] \\ & R_2 = \frac{v}{rw}\left[u_\eta-v\right] \\ & R_3 = \frac{\Delta}{r}\left[-\mathcal{J}vP_\eta-a^2(v_\xi\xi_\theta+v_\eta+u)+vww_\eta\right] \end{aligned}\right. \tag{31}$$

V. BODY POINTS

To inforce the boundary condition at the body, the same technique used in Refs. 11 and 12 will be applied. Eq. (30), written with X,Y and Z in lieu of $\xi, \eta,$ and θ, is made explicit with respect to P_Z. The third equation from (25), (26) is used to obtain v_Z. After updating v and P, $\mathcal{J}$ can be computed since S is a constant on the body, using the equation:

$$\mathcal{J} = \exp\left[\frac{\gamma-1}{\gamma} P + \frac{1}{\gamma} S\right] \tag{32}$$

Then, the square of the modulus of the velocity, q^2 is obtained from the law of conservation of total energy:

$$q^2 = 2\left[\frac{\gamma}{\gamma-1} + \tfrac{1}{2}V_\infty^2 - \frac{\gamma}{\gamma-1}\mathcal{J}\right] \tag{33}$$

and the two velocity components, u and w, follow from the condition of vanishing of the velocity component normal to the body:

(34) $$w = \frac{1}{1+b_z^2}\left[-\frac{b_\theta}{b} b_z v + \sqrt{(q^2-v^2)(1+b_z^2)-\left(\frac{b_\theta}{b}\right)^2 v^2}\right]$$

(35) $$u = \frac{b_\theta}{b} v + b_z w$$

VI. SHOCK POINTS

The shock points will also be treated by the same technique used in Refs. 11 and 12. In the present problem, however, two changes have to be made: the impinging velocity is simply parallel to the z-axis, and the shock is not the Z=1 boundary of the computational region. Let $\hat{i}$, $\hat{j}$, and $\hat{k}$ be unit vectors in the directions of increasing r, increasing θ, and increasing z, respectively, $\hat{I}$ a unit vector normal to the shock, oriented inwards, and $\hat{K}$ a unit vector tangent to the shock and contained in a meridional plane. Let $s(\theta,z)$ be the r-coordinate of a point on the shock, and $\tilde{u}$ the velocity component in the $\hat{I}$-direction. Finally, let ζ be a coordinate along $\hat{K}$. Then,

(36) $$\vec{V}_\infty = V_\infty \hat{k}$$

(37) $$I = [-\hat{i}+(s_\theta/s)\hat{j} + s_z\hat{k}]/\nu = I_1\hat{i}+I_2\hat{j}+I_3\hat{k}$$

(38) $$\nu = \sqrt{1+(s_\theta/s)^2+s_z^2}$$

(39) $$\tilde{u}_\infty = V_\infty I_3$$

The Rankine-Hugoniot conditions yield

(40) $$P = \ln \frac{2\tilde{u}_\infty^2-(\gamma-1)}{\gamma+1}$$

(41) $$\tilde{u} = \frac{\gamma-1}{\gamma+1}\tilde{u}_\infty + \frac{2\gamma}{\gamma+1}\frac{1}{\tilde{u}_\infty}$$

where P and $\tilde{u}$ are values behind the shock. Since the Rankine-Hugoniot conditions are identically satisfied along the shock, it follows that

(42) $$P_\zeta = \frac{4\tilde{u}_\infty}{2\tilde{u}_\infty^2-(\gamma-1)}\tilde{u}_{\infty\zeta}$$

(43) $$\tilde{u}_\zeta = \left[\frac{\gamma-1}{\gamma+1} - \frac{2\gamma}{\gamma+1}\frac{1}{\tilde{u}_\infty^2}\right]\tilde{u}_{\infty\zeta}$$

In addition, if we write

$$\vec{V}_\infty = \tilde{u}_\infty \hat{I} + \vec{\tilde{v}} \tag{44}$$

it follows that, behind the shock,

$$\vec{V} = \tilde{u}\,\hat{I} + \vec{\tilde{v}} = \vec{V}_\infty + (\tilde{u}-\tilde{u}_\infty)\hat{I} \tag{45}$$

From (45),

$$\left\{\begin{aligned} u_\zeta &= (\tilde{u}-\tilde{u}_\infty)_\zeta I_1 + (\tilde{u}-\tilde{u}_\infty) I_{1\zeta} \\ v_\zeta &= (\tilde{u}-\tilde{u}_\infty)_\zeta I_2 + (\tilde{u}-\tilde{u}_\infty) I_{2\zeta} \\ w_\zeta &= (\tilde{u}-\tilde{u}_\infty)_\zeta I_3 + (\tilde{u}-\tilde{u}_\infty) I_{3\zeta} \end{aligned}\right. \tag{46}$$

Now,

$$\tilde{u}_{\infty\,\zeta} = V_\infty I_{3\zeta} \tag{47}$$

The derivatives $I_{1\zeta}$, $I_{2\zeta}$, and $I_{3\zeta}$ can be evaluated by differentiating (37). After some algebraic manipulations, it follows that

$$\left\{\begin{aligned} u_\zeta &= E_1 I_1 + E_2 s_{zz} \\ w_\zeta &= E_1 I_3 + E_3 s_{zz} \\ P_\zeta &= E_4 + E_5 s_{zz} \end{aligned}\right. \tag{48}$$

with

$$\begin{aligned} E_1 &= -\frac{4}{\gamma+1}\tilde{u}_\infty C_1 I_1 I_2 \\ E_2 &= -\tilde{u}_\infty I_1^2 [C_2 V_\infty/\tilde{u}_\infty + \frac{4}{\gamma+1} I_3] \\ E_3 &= \frac{4}{\gamma+1}\tilde{u}_\infty I_1 (1-I_3^2) \\ E_4 &= -C_2 C_1 \tilde{u}_\infty I_3/\nu_1 \\ E_5 &= C_3 (V_\infty - \tilde{u}_\infty I_3)/\nu_1 \\ C_1 &= (s_{\theta z} - s_\theta s_z/s)/s \\ C_2 &= -\frac{2}{\gamma+1}(1+\gamma/\tilde{u}_\infty^2) \\ C_3 &= \frac{4\tilde{u}_\infty}{2\tilde{u}_\infty^2 - (\gamma-1)} \\ \nu_1 &= \sqrt{1+(s_\theta/s)^2 + s_z^2} \end{aligned} \tag{49}$$

Eq. (30) is used as written, with $\zeta=1$. The derivatives, P_ζ, u_ζ, and w_ζ are replaced by (48) and the unknown s_{zz} car be made explicit as follows:

$$(50)\qquad s_{zz}=-\frac{\mu_1(E_4+\lambda P_\zeta+R_1)+\mu_2(E_1I_1+\lambda u_\zeta+R_2)+\mu_3(E_1I_2+\lambda w_\zeta+R_3)}{\mu_1E_5+\mu_2E_5+\mu_3E_5}.$$

The quantity s_{zz} is used to update s_z and this, in turn, to update s. Once the updated geometry of the shock is known, all physical parameters behind the shock follow from the Rankine-Hugoniot conditions.

VII. ORGANIZATION OF A COMPUTATIONAL STEP

At any station, z, the computational region in the (X,Y) frame is a rectangle (Fig. 3) whose horizontal sides represent the body and the outer boundary, and whose vertical sides represent two symmetry lines, at $\theta=0$ and $\theta=\pi/2$ (in the present calculation, obviously, one quadrant is sufficient to describe the entire region around the body). The shock (whose cross-section in case 1 and case 2 is really circular) appears in the computational region as a curve, whose shape depends on the geometry of the outer boundary.

All vertical lines in the grid of Fig. 3 correspond to meridional planes. Shock points will be tracked along such lines, as shown in the figure.

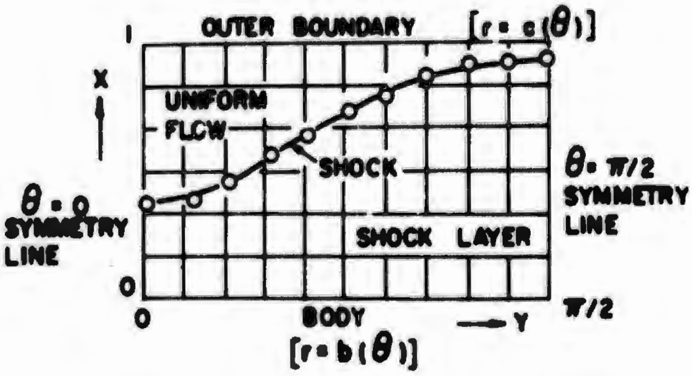

Fig. 3

Any computational step consists of three parts:

1) an introduction, to evaluate the step size satisfying the Courant-Friedricks-Lewy condition,

2) a predictor stage, and

3) a corrector stage.

Both the predictor and the corrector stages use the same code with minor changes. First, the shock is computed. Eq. (50) is used to get s_{zz}. Without changes in coding, predictor and corrector stages will automatically use different values for the right-hand side of (50); in the predictor stage all initial values and initial geometries will be used, in the corrector stage all predicted values and updated geometries will be used.

In the predictor stage, s_z and s are obtained as

$$(s_z)_{pred} = (s_z)_{initial} + s_{zz}\Delta z \tag{51}$$

$$s_{pred} = s_{initial} + (s_z)_{initial}\Delta z \tag{52}$$

In the corrector stage, s_z and s are obtained as

$$s_z = \tfrac{1}{2}[(s_z)_{initial} + (s_z)_{pred} + s_{zz}\Delta z] \tag{53}$$

$$s = \tfrac{1}{2}\{s_{initial} + s_{pred} + \tfrac{1}{2}[(s_z)_{initial} + s_z]\Delta z\} \tag{54}$$

In both stages, after updating all shock points, the new geometry is used to obtain I and then $\tilde{u}_{\infty}$, P and $\tilde{u}$ follow from (39), (40), and (41).

After computing the shock, in both stages, the ordinary mesh points are computed. As a rule, (25) is integrated by the Mac Cormack scheme.[14] Forward and backward differences are used in the predictor and in the corrector stage, respectively.

Exceptional points are:

a) body points

b) outer boundary points

c) points in the vicinity of the shock.

Outer boundary points are not computed at all since they always lie in a region of uniform, unperturbed flow.

At body points, (30) is used to obtain P, and the remaining physical parameters are computed as explained in Section 5.

Points in the vicinity of the shock are computed as ordinary points as long the interval on which the finite difference is taken does not intersect the shock. If intersection occurs, the derivatives will be evaluated differently, as explained in the next Section.

All these points are computed in the predictor stage. At the end of the stage, the geometry of the body and of the outer boundary is updated; a new search of "points lying in the vicinity of the shock" is performed, with the shock in its updated position. Then all the interior points and body points are recomputed in the corrector stage.

VIII. SPECIAL APPROXIMATIONS OF DERIVATIVES

Section 7 exhausts the entire logic of the computation; with all points, except shock points, computed similarly and the predictor and corrector stages programmed in a single loop, the code is indeed simple and short. Its only delicate feature is the discretization of the X-and-Y-derivatives at body points and at points in the vicinity of the shock, as well as of the ξ-and-η-derivatives at shock points.

At body points, if one-sided X-differences are used in both predictor and corrector stage, the pressure tends to become slightly lower than at the adjoining row; a result which is definitively incorrect, as a comparison with the exact solution shows. Taking one-sided differences in the predictor stage is in agreement with the code for interior points. In the corrector stage, however, I prefer to use 3-point differences, of the form

(55) $$f_X \approx (-1.5f_1+2f_2-.5f_3)/\Delta X$$

where 1,2,3 denote points on the body and the two successive rows, in order.

At shock points, η-derivatives will simply be approximated by centered differences of shock point values (note that the shock points are equally spaced in θ). More delicate is the treatment of ξ-derivatives. Following the suggestion of page 70, Ref. 4 and particularly the procedure expressed by Eq. (100), I use here the formula:

(56) $$f_X = [1.5f_Q-2\epsilon f_P-(2-2.5\epsilon)f_R+.5(1-\epsilon)f_S]/\Delta X$$

where

(57) $$\epsilon = \frac{X_Q-X_P}{\Delta X}$$

and Q,P,R, and S denote values at the shock and at the 3 mesh points lying on the same X-line as the shock point on the high-pressure side, for decreasing values of X (Fig. 4). To get the ξ-derivative, note that

(58) $$f_\xi = f_X X_\xi = f_X X_r/\xi_r = f_X X_S$$

where X_S is the value of X at the shock point.

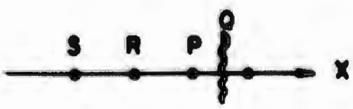

Fig. 4

Points in the vicinity of the shock (denoted by a double circle in Fig. 5) have at least one of the adjoining mesh intervals crossed by the shock (as shown in Fig. 5 where the shock is denoted by a waving line). If only one mesh interval is crossed, the point is labeled as shown in Fig. 5.

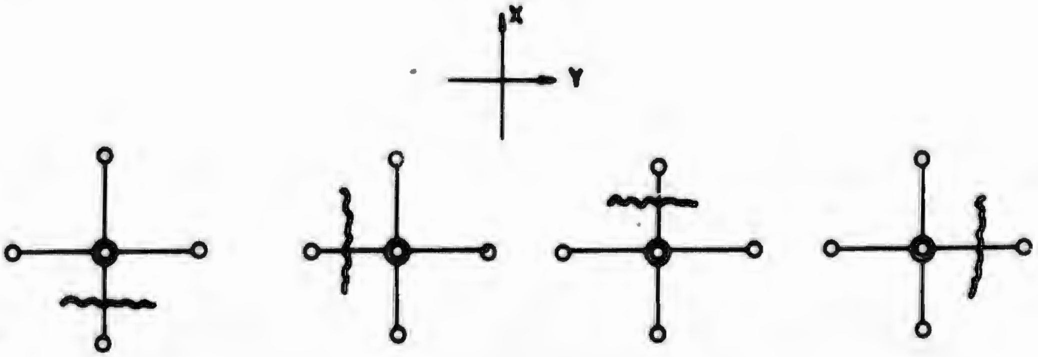

FOR LOW PRESS. SHOCK	1	10	100	1000
FOR HIGH PRESS. SHOCK	2	20	200	2000

Fig. 5

If more than one mesh interval is crossed by a shock, corresponding labels are added, so that for any possible situation a four digit label describes the nature of the point. Examples are given in Fig. 6.

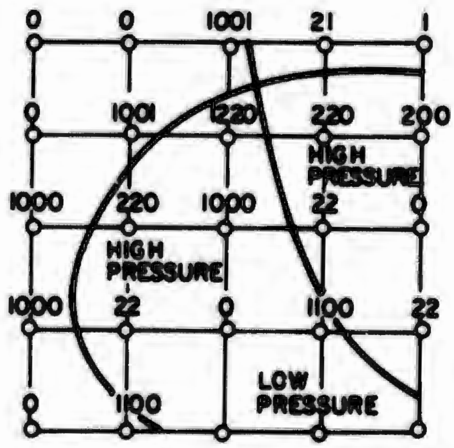

Fig. 6

In the present problems, with only one shock, the situation is never as complicated as in Fig. 6, but the example is given to show the advantages of a four-digit label. It is clear that, by scanning the label of each mesh point, each non-zero digit may divert the computation of f_X or f_Y to a special code, using information on one side of the shock only, when the usual procedure would imply differences between points lying on opposite sides of the shock. Note also that each digit works independently; therefore, complicated situations such as the ones shown in Fig. 6 are resolved into simple routines.

With X and Y as in Fig. 5, in the predictor stage f_X has to have a special definition for points labeled 100 and 200, f_Y for points labeled 1000 and 2000. In the corrector stage, the special treatment is reserved for points labeled 1 and 2, and 10 and 20, respectively.

The X-derivative at P is obtained as follows: Let $f_X^{(1)}$ and $f_X^{(2)}$ be two approximations to f_X, the first obtained by forward differencing between point P and the adjacent shock point (Q):

$$f_X^{(1)}=(f_Q-f_P)/\epsilon\Delta X \tag{59}$$

the second linearly interpolated between the derivative at Q given by (56) and the forward-difference approximation to the derivative at R:

$$f_{XQ}=(f_P-f_R)/\Delta X + (1+\epsilon)[f_X^{(2)}-(f_P-f_R)/\Delta X] \tag{60}$$

We will use the approximation:

$$\begin{aligned} f_{XP} &= \epsilon f_X^{(1)}+(1-\epsilon)f_X^{(2)} \\ &= [f_Q-(1-\alpha)f_P-\alpha f_R]/\Delta X+\beta f_{XQ} \end{aligned} \tag{61}$$

where

$$\beta = \frac{1-\epsilon}{1+\epsilon} \quad , \quad \alpha=\epsilon\beta \tag{62}$$

, similar formula may be obtained for points Q, P, R, S located in the order opposite to the one of Fig. 4.

The Y-derivative at a point labeled 1000 or 2000 is obtained by applying the same argument to the Y-coordinate. In this case, the values at Q are not directly available since point Q lies at the intersection of the shock with an X=constant line and shock points are evaluated only at the intersection of the shock with Y=constant lines. Therefore, the values at Q are obtained by linear interpolation between values at bracketing shock points.

Note also that, occasionally, the shock may cut an X=constant line twice as shown in Fig. 7.

Fig. 7

If f_Y has to be computed at P, in the case of Fig. 7a) (61) can still be used, but (56) cannot, since point S lies on a different side of the shock as Q, P, and R. To evaluate f_{YQ} in this case I use the formula:

(63) $$f_{YQ}=[d_1 f_P+d_2 f_R+d_3 f_Q+d_4 f_B]/\Delta Y$$

where

(64)
$$d_1=-(1+\epsilon)$$
$$d_2=\frac{\epsilon^2}{1+\epsilon}+1-\epsilon-\frac{1-\epsilon}{1+\epsilon+\eta}\left(\frac{\eta^2}{1+\epsilon}+3\eta+2+2\epsilon\right)$$
$$d_3=\frac{1+2\epsilon}{1+\epsilon}+\frac{1-\epsilon}{1+\epsilon+\eta}\left(\frac{\eta^2}{1+\epsilon}+1+\eta\right)$$
$$d_4=-1+\epsilon-\frac{1-\epsilon}{1+\epsilon+\eta}(1-2\eta-2-2\epsilon)$$

(65)
$$\epsilon=(Y_Q-Y_P)/\Delta Y$$
$$\eta=(Y_R-Y_B)/\Delta Y$$

This formula is obtained by balancing a three-point interpolation formula which uses points Q, P, and R, a three-point interpolation formula which uses points Q, R, and B and a difference on points Q and B; the first provides a derivative $f'_{(1)}$, the second a derivative $f'_{(2)}$ and the third a derivative $f'_{(3)}$; then

(66) $$f_{YQ} = \epsilon f'_{(1)} + (1-\epsilon)\left[\eta f'_{(2)} + (1-\eta) f'_{(3)}\right]$$

By so doing, the values of f_{yQ} are well-behaved even if ϵ or η become very small, that is, when the shock at Q or at B is about to cross from one mesh interval to the next. A similar formula is used for the derivative at B in the case of Fig. 7a).

In the case of Fig. 7b) the derivative at P is simply taken as

(67) $$f_Y = \frac{f_Q - f_B}{Y_Q - Y_B} .$$

IX. RESULTS FOR CASE 1

Runs were made for a 27° cone, at $M_\infty = 2.5$, using $b_1 = 0.5$, $c_1 = 1.0$. The slope of the outer boundary was chosen as follows:

Run No.	12	$\tau = 2.7$
	13	2.5
	14	2.0
	15	1.5

The number of mesh intervals between body and outer boundary was kept equal to 15 for all runs. Since the flow is actually axisymmetric, only one interval (with $\Delta\theta = \pi/2$) was considered in the computational quadrant. Sideviews of the cone, the theoretical shock and the outer boundary are shown in Fig. 8, together with some of the mesh lines.

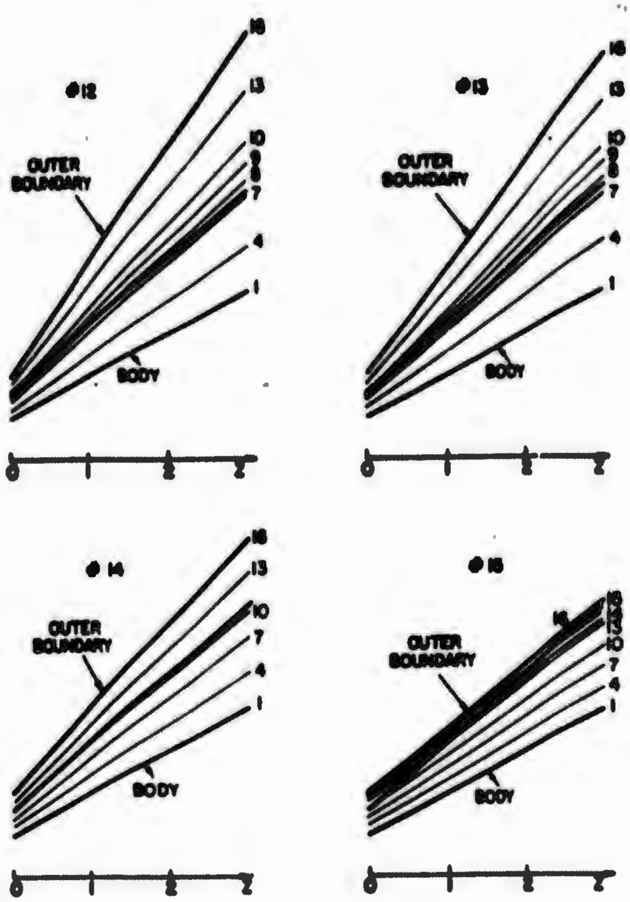

Fig. 8

It appears that in Runs No. 12 and 13 the shock crosses mesh lines inwardly and in Run No. 15 the shock crosses mesh lines outwardly, whereas in Run No. 14 no crossing occurs. Difficulties and instabilities due to meshline crossing should appear differently in these four runs, showing how the accuracy is influenced and perhaps damaged by different choices of computational parameters.

Nothing of the sort occurs, though, as we can see from Fig. 9, which provides the history of P at the shock in all four runs, for 60 computational steps. In each run, the station at which a crossing of the mesh lines occurs is indicated by a vertical arrow (pointing downwards if the crossing is in the inward direction and upwards if the crossing is in the outward direction). It is evident that the computation is totally insensitive to mesh line crossing.

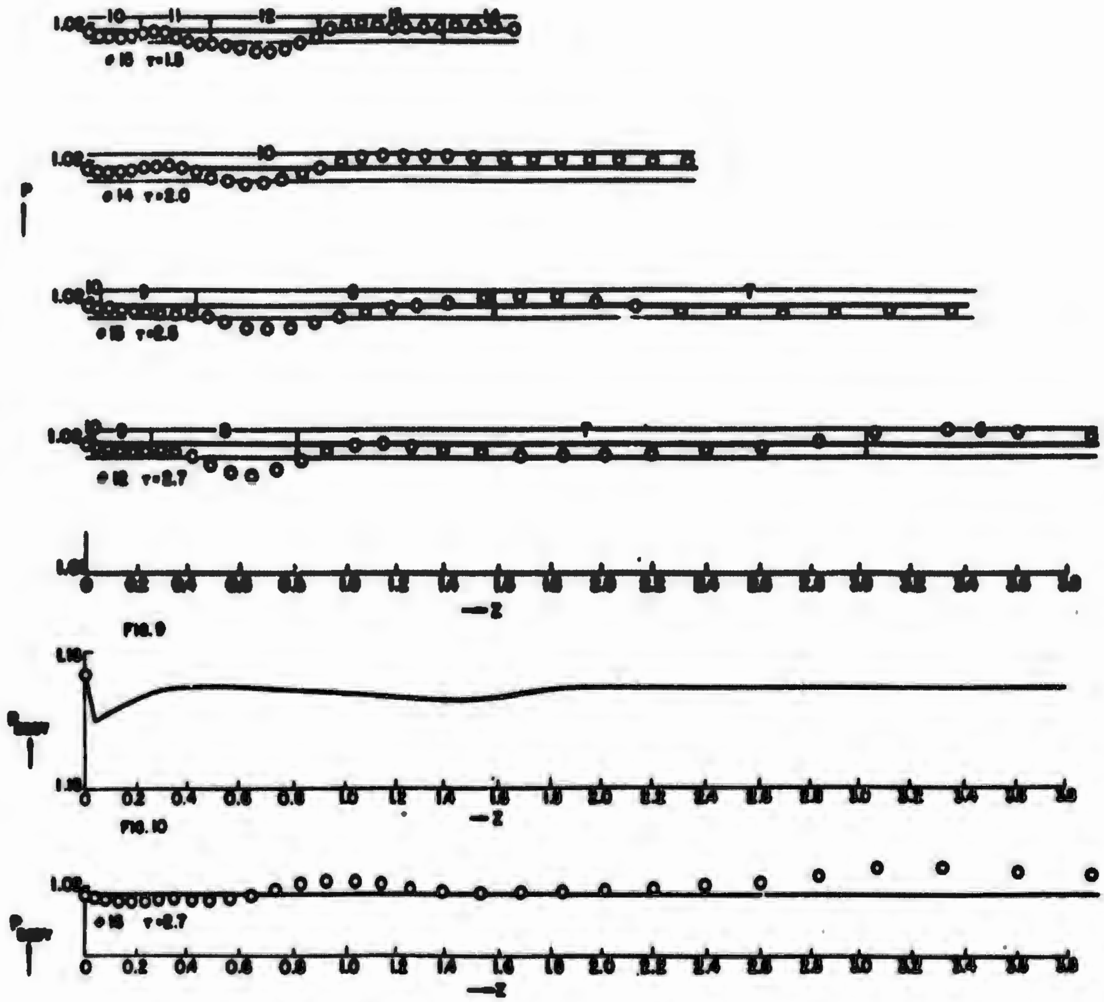

FIG. 11

An interesting feature of all four plots is a slight dip in the shock pressure between z=.4 and z=1.0 approximately. Obviously, the dip is not mesh dependent. It is, instead, produced by the physical propagation of an expansion fan generated at the body between z=0 and z=0.05, followed by a recompression, as shown by the plot of P(z) on the body in Fig. 10 and probably due to some initial inconsistency between the assumed "exact" solution and the finite difference algorithm. To prove that the oscillation is actually an effect of the initial expansion at the body, Run 16 was made under the same conditions as Run 12, but forcing the pressure at the body to remain constant. Fig. 11 shows that the depression at the shock also disappears.

I consider the results very satisfactory. To show some deviation from the exact solution, I had indeed to make sure of a fairly small scale for P. In Fig. 9, above and below each horizontal line representing the theoretical pressure at the shock, there are two more horizontal lines defining a strip of 0.001 accuracy. With the exception of the initial dip, which has its own explanation, all results lie within the strip. To fully appreciate the power of stability and accuracy of the computation, one should also keep in mind the coarseness of the mesh. Although 15 mesh intervals are considered between body and outer boundary, not all of them lie in the shock layer. The number of mesh points between body and shock is indicated in Fig. 9 by the numbers above each exact solution line. Run 12, for example, disposes of only 6 points for z>3; it is obviously bound to a poorer accuracy than Run 15 which, at z=1.4, has already 14 mesh points. That lack of resolution is

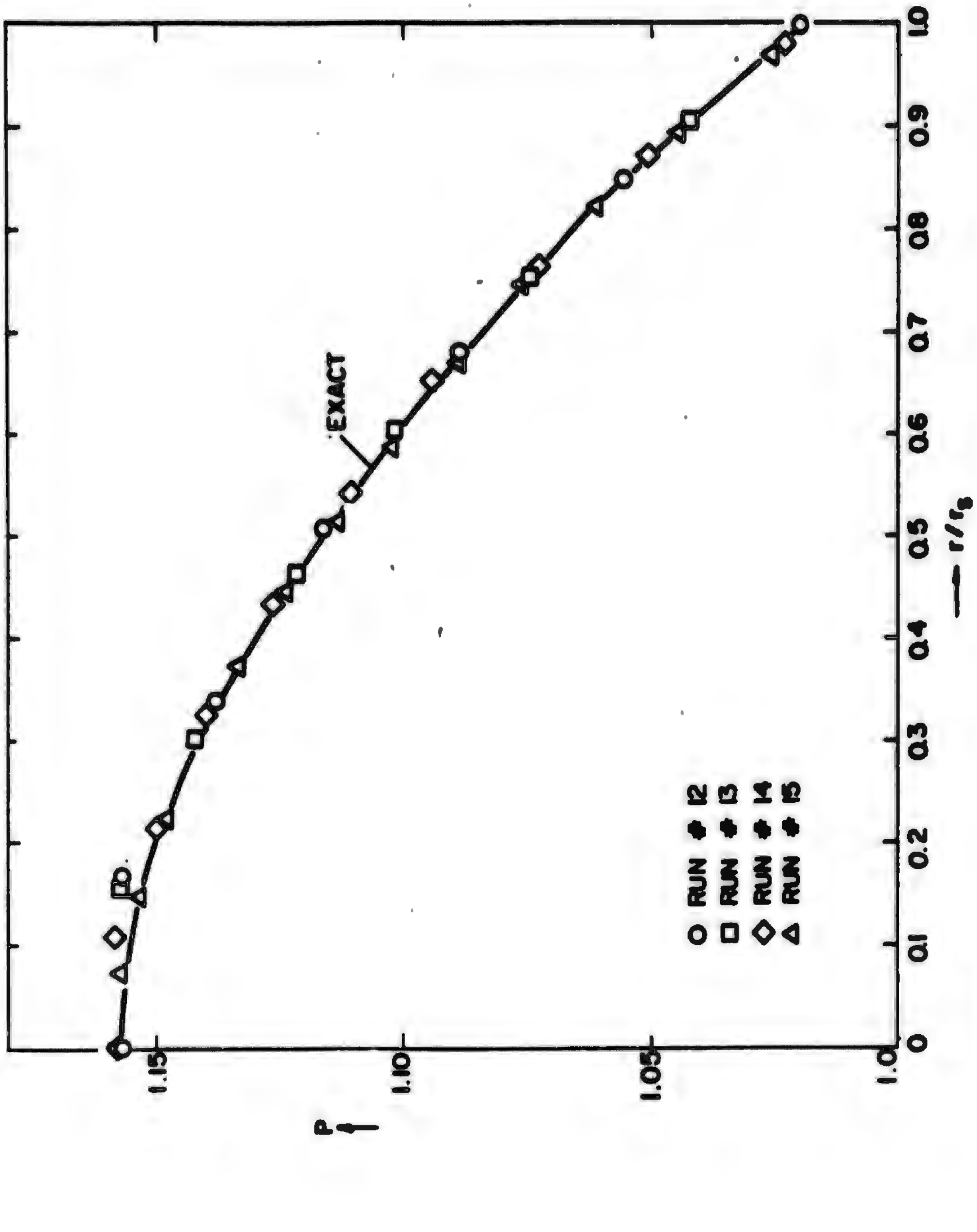
P
1.15
1.10
1.05
1.0
0
0.1
0.2
0.3
0.4
0.5
0.6
0.7
0.8
0.9
1.0
r/rs
EXACT
RUN # 12
RUN # 13
RUN # 14
RUN # 15

FIG. 12

not affecting the computation of the shock, but rather influencing the computation at the body, is well shown by Fig. 12 where, for the four runs, at step 60, pressure distributions between body and shock are plotted, together with the exact value, on a normalized scale.

X. RESULTS FOR CASE 2

In case 2, we still deal with the same cone as in case 1, but the outer boundary has a variable elliptic cross-section, defined by

$$\tau=2.7 \quad , \quad \sigma=1.5$$

By comparison with the data of runs 12 and 15, we see that the shock will tend to cross mesh points inwardly at $\theta=\pi/2$ and outwardly at $\theta=0$. Fig. 13 shows a typical cross-section to be expected at z=3. We should obtain the same results as in the previous case, that is, a conical shock layer, in a mesh which is not axially symmetrical.

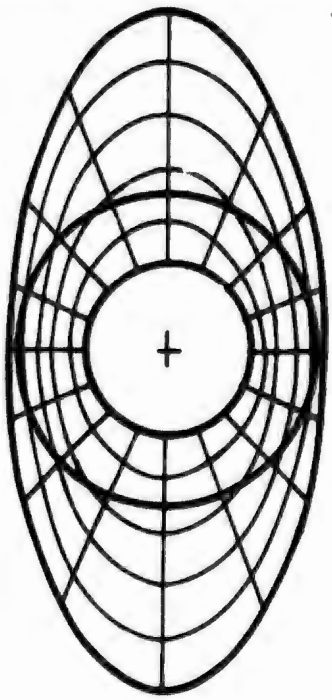

Fig. 13

Fig. 14 shows the minimum and maximum values of P at the shock, for increasing values of z, in four different runs. The bottom of the figure corresponds to a computation in which the body is evaluated according to Section 5; Run 21 is a computation where the body pressure is kept constant (a condition which can be imposed since the flow is still axisymmetric). Both runs were made with 15 mesh intervals in the radial direction and 9 intervals (10° wide) in the θ-direction. Run 24 is a computation using 18 intervals (5° wide) in the θ-direction. Once more we find that the scattering of values remains in the 0.001 strip and it is comforting to see that the accuracy tends to improve by using more intervals in the θ-direction. Even better accuracy is shown by Run 28 (top of Fig. 14), a computation which uses 25 intervals in the X-direction and 18 intervals in the Y-direction. Here the maximum scattering is of the order of 4×10^{-4}.

Fig. 14 is the presentation of results by the devil's advocate. A more conventional plot is given in Fig. 15 where the pressure distribution between body and shock is presented, as computed at the last station of Run 21. Once more, as in Fig. 12, the distance between shock and body is normalized. The solid line is the exact solution. Different symbols denote values computed at different meridional planes. The only sizeable departures from the exact solution is near the body and obviously decreasing with increasing resolution.

Fig. 16 shows the computational mesh and the location of the shock in the physical plane at the last station of Run 21.

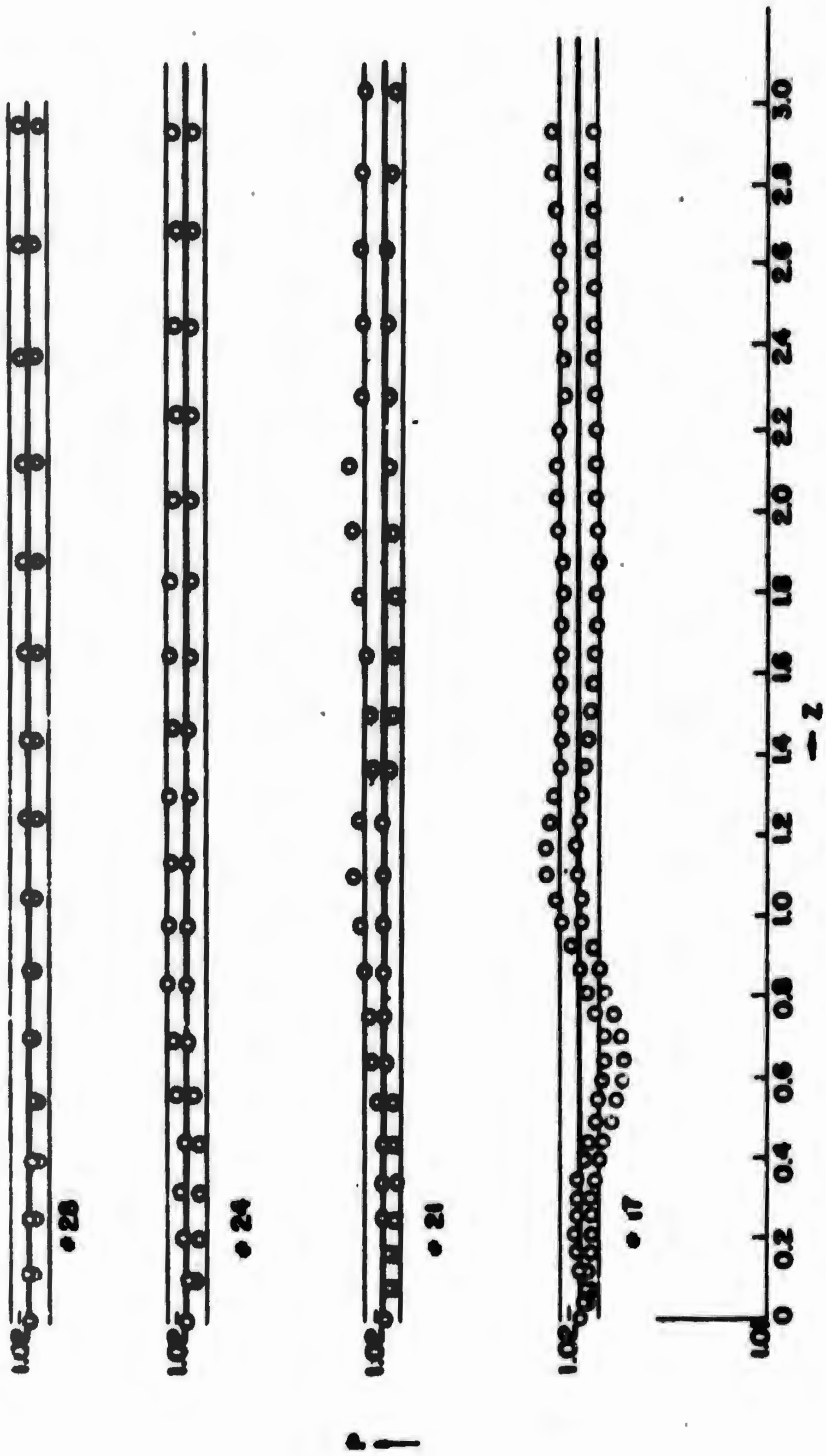

ϕ 28
ϕ 24
ϕ 21
ϕ 17
1.02
1.00
0
0.2
0.4
0.6
0.8
1.0
1.2
1.4
1.6
1.8
2.0
2.2
2.4
2.6
2.8
3.0
Z

FIG. 14

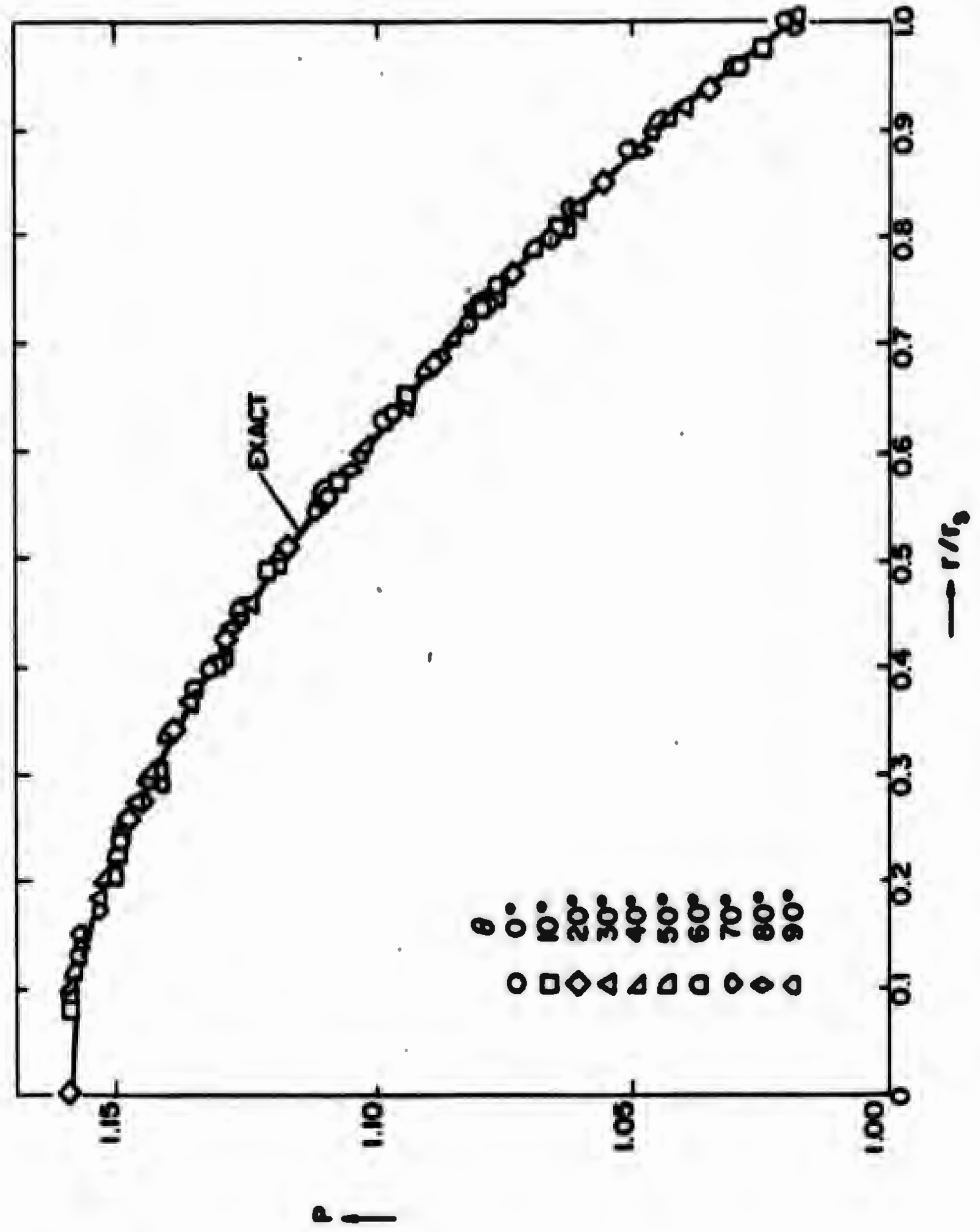

EXACT
θ
0°
10°
20°
30°
40°
50°
60°
70°
80°
90°
1.15
1.10
1.05
1.00
P
0
0.1
0.2
0.3
0.4
0.5
0.6
0.7
0.8
0.9
1.0
r/r_s

FIG. 15

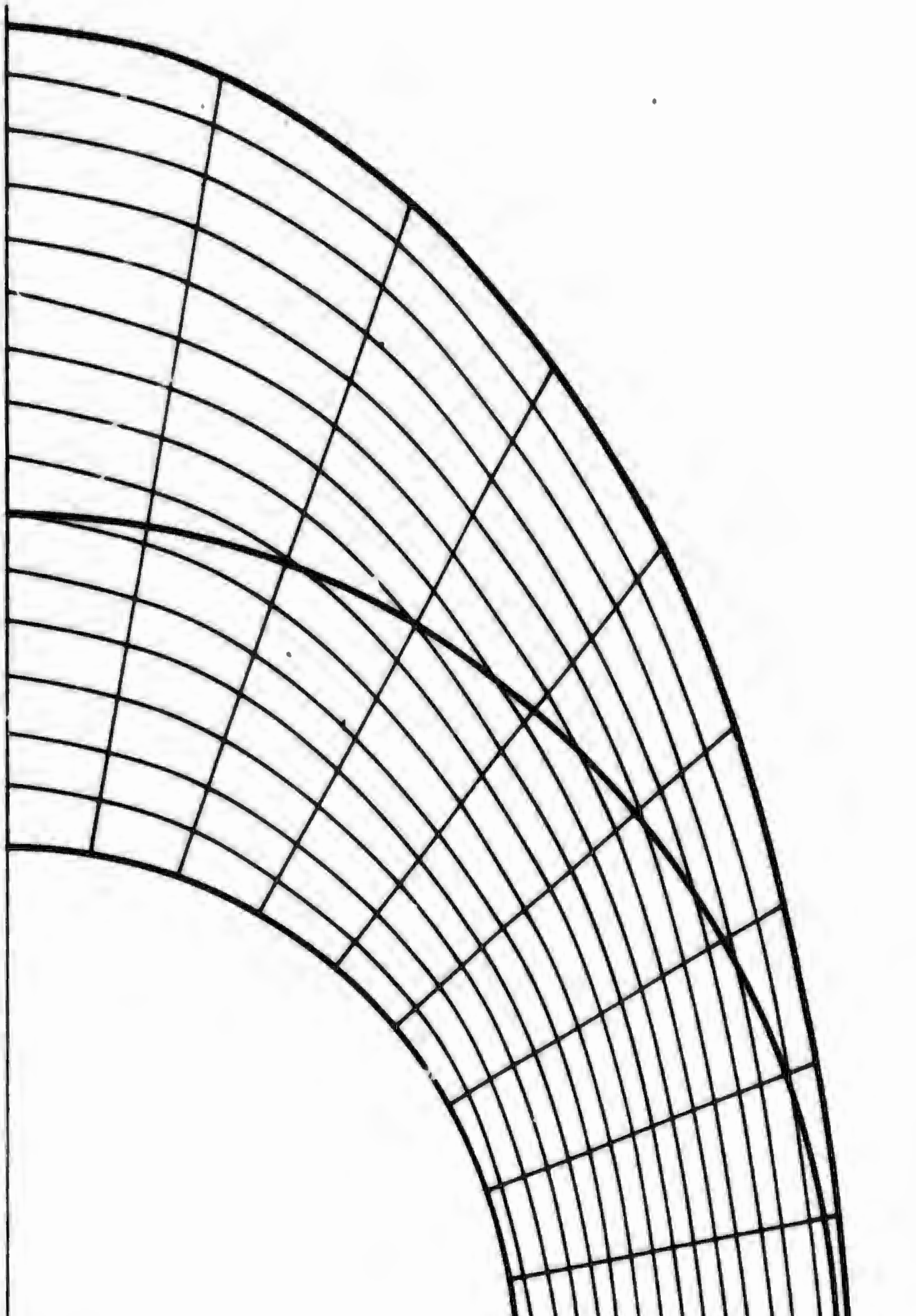

FIG. 16

In Fig. 17 the mesh and the shock are shown in the computational (X,Y) plane at the same station. Labels for the points neighboring the shock, as evaluated by the computer, are also shown.

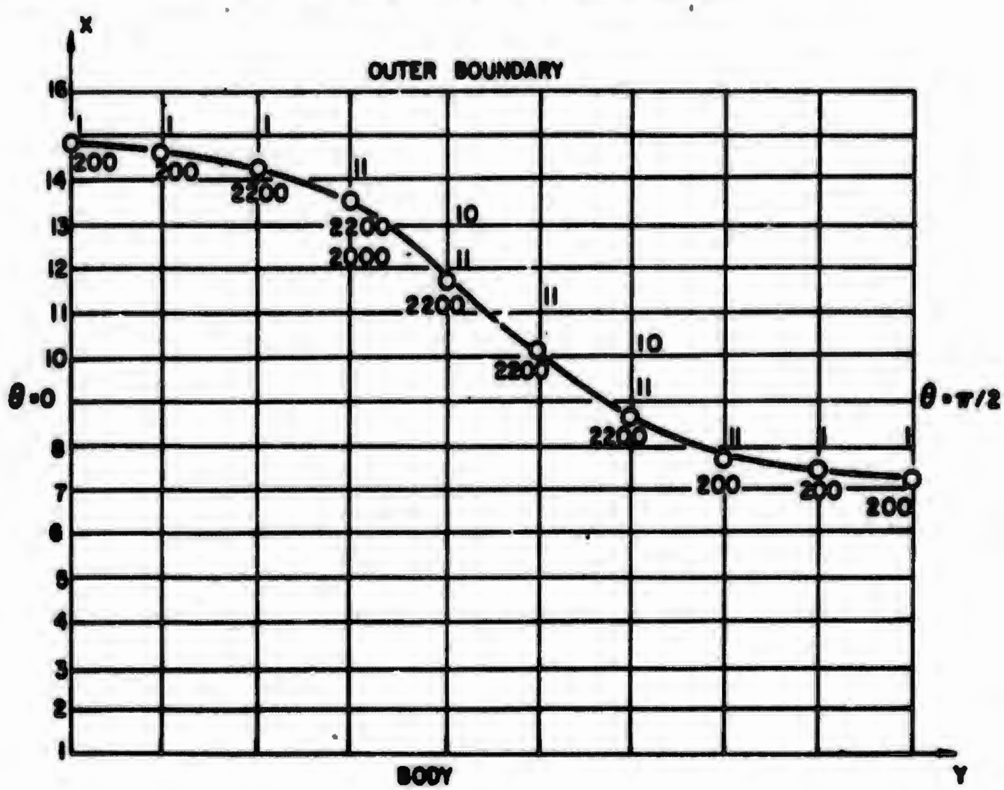

Fig. 17

XI. RESULTS FOR CASES 3 AND 4

In cases 3 and 4 the intersection of the body with the $\theta=\pi/2$ plane tapers down to the constant value, r=1, and maintains it from $z=z_o=3$ on. The body assumes the shape of a delta wing with an elliptic cross-section. In case 3, the outer boundary grows as a circular cone. In case 4, it has an elliptical cross-section with its major and minor axes at 90^o with respect to the major and minor axes of the body cross-section, to twist the computational mesh as much as possible. The mesh, in both cases, has 15 intervals in the X-direction and 9 intervals in the Y-direction; it is, though, a very coarse mesh, as it can be seen in

Figs. 18 and 19. In particular, one may notice the extreme lack of resolution between θ=0 and θ=10°. Another shortcoming of the calculations stems from the abrupt expansion and recompression taking place near the body; such effect, due to the rapid change in the body geometry, tends to produce a cross-flow shock at z=10, long before sizeable effects of the expansion at the body have a chance of influencing the shock drastically. Of course, since no provision for the crossflow shock is made, the results in the vicinity of the body, between θ=20° and θ=40° become wild and the computation stops. Nevertheless, the entire flow field is definitively three-dimensional, and the shock itself is no longer circular in cross-section, so that we may say that in both cases we are dealing with a three-dimensional problem, where all derivatives are different from zero, and, moreover, in a computational mesh which is the most unfitted to make the computation easy. The results are very encouraging. Despite several crossings of mesh line by the shock, in all directions, the shock develops in a stable way and appears very smooth. The pressure distribution within the shock layer is very good, except where the cross-flow shock should build up. This is shown by the isobar pattern of Fig. 18. The isobar pattern is not shown in Fig. 19 because it is exactly the same as in Fig. 18, despite the difference in the mesh and in the location of the shock relative to the mesh. Note also that the crowded isobar pattern near the body in the shadowed region of Fig. 18 has been omitted. Fig. 20 shows the location of the shock in the (X,Y) plane and the distribution of labels at the last computed station in Case 4, Run 27.

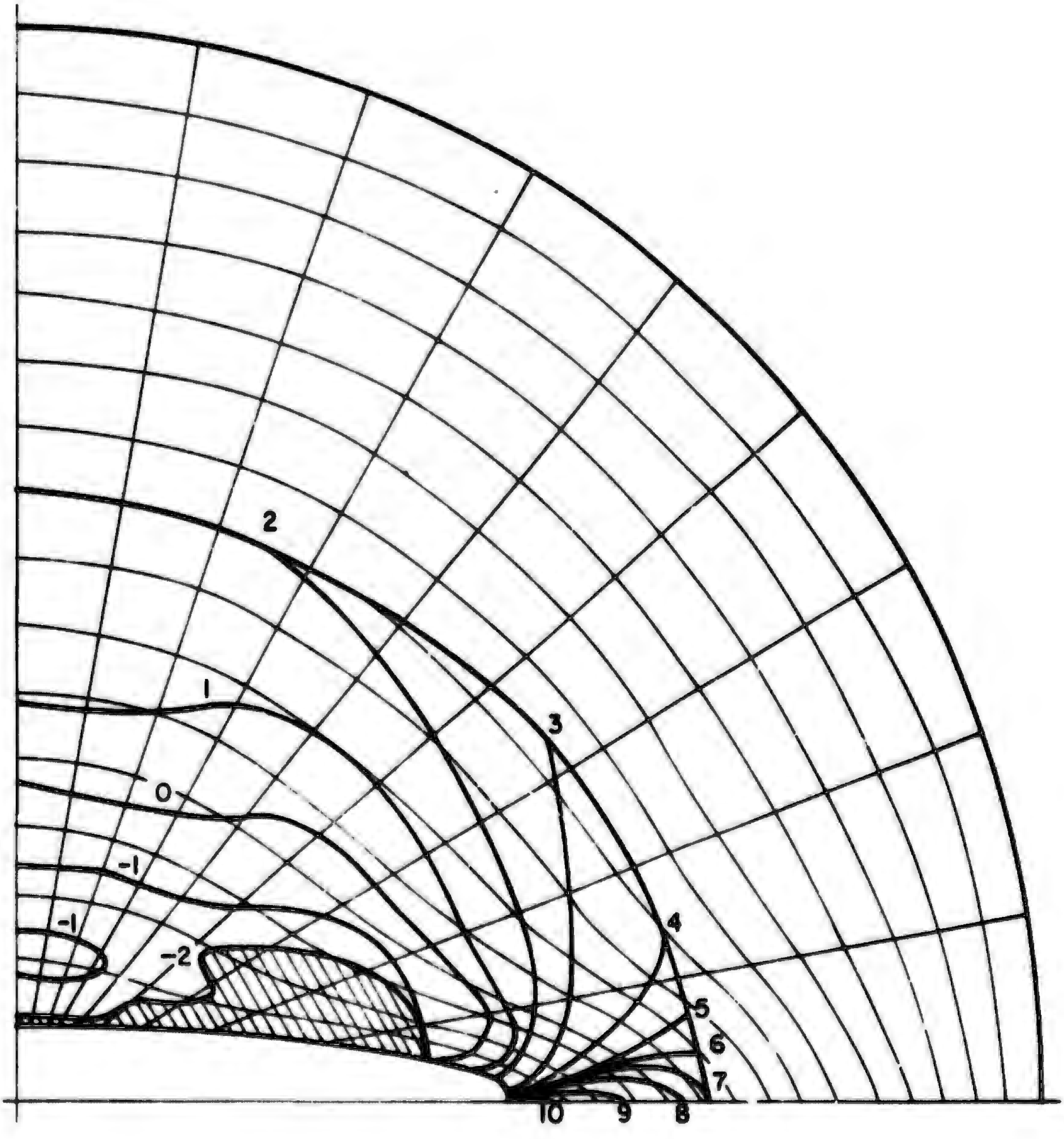

FIG. 18

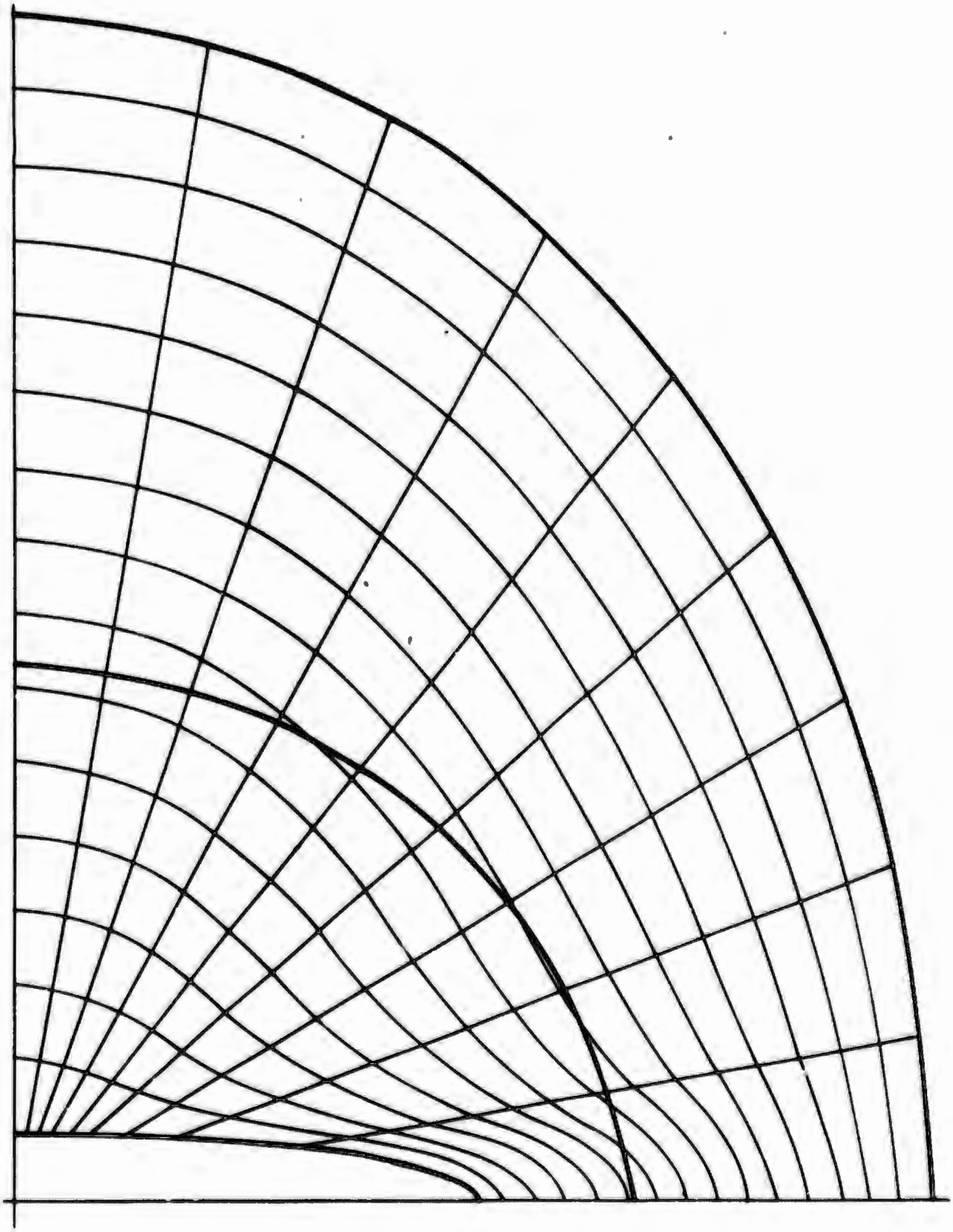

FIG. 19

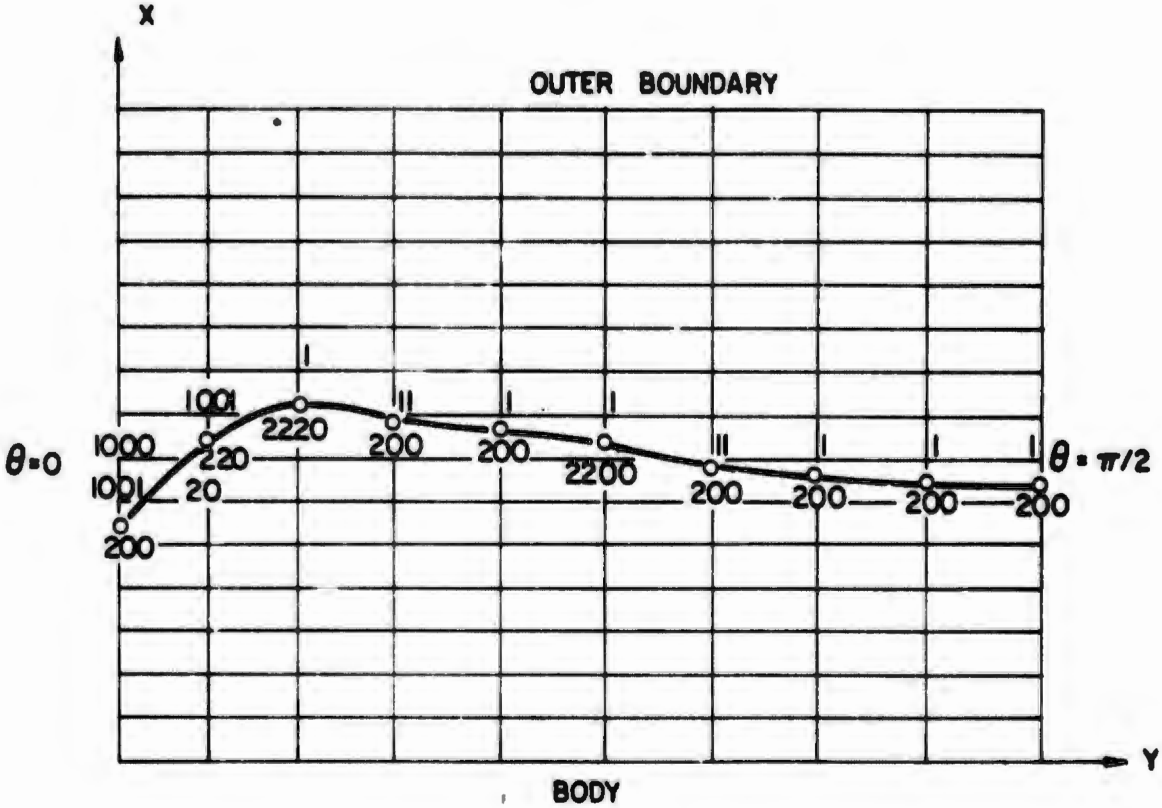

Fig. 20

XII. CONCLUSIONS

Computations of three-dimensional, supersonic, steady flows with shocks floating among mesh points can be performed. The results so far obtained are stable and mesh-independent. The logic necessary to handle such shocks is simple. Extension of the technique exposed in the present Report to cases where shocks may appear in all directions will require some reformulation of the shock equations which, so far, depend too heavily on the shock being defined by (29). Some additional bookkeeping will also be required to account for the presence of multiple shocks.

The basic principles, however, will stand as stated in this Report and most of the equations will be usable without changes, in particular the crucial approximations for derivatives at points neighboring a shock (which, so far, allow the computation to remain stable). Extensions of the sort and applications as mentioned in the introduction are surely worthwhile since the present technique can produce very accurate results with a minimum of mesh points, that is, using a computer at peak efficiency.

XIII. REFERENCES

1. Moretti, G.: A Critical Analysis of Numerical Techniques: The Piston-Driven Inviscid Flow. Polytechnic Institute of Brooklyn, PIBAL Report No. 69-25, AD 693037, July 1969.
2. Moretti, G.: The Choice of a Time-Dependent Technique in Gas Dynamics. Polytechnic Institute of Brooklyn, PIBAL Report No. 69-26, AD 705514, July 1969.
3. Moretti, G.: Complicated One-Dimensional Flows. Polytechnic Institute of Brooklyn, PIBAL Report No. 71-25, AD 731494, September 1971.
4. Moretti, G.: Thoughts and Afterthoughts About Shock Computations. Polytechnic Institute of Brooklyn, PIBAL Report No. 72-37, AD 760015, December 1972.
5. Moretti, G.: Computations of Complicated Steady Supersonic Flows in Two-Dimensional and Axisymmetric Ducts. Polytechnic Institute of New York; to be issued as a PIBAL report.

6. Grossman, B. and Moretti, G.: Time-Dependent Computation of Transonic Flows. Presented at the AIAA 7th Annual Meeting and Technical Display, Houston, Texas, October 19-22, 1970, AIAA Paper 70-1322.

7. Moretti, G., Grossman, B., and Marconi, F., Jr.: A Complete Numerical Technique for the Calculation of Three-Dimensional Inviscid Supersonic Flows. Presented at the AIAA 10th Aerospace Sciences Meeting, San Diego, California, January 17-19, 1972, AIAA Paper No. 72-192.

8. Marconi, F. and Salas, M.: Computation of Three-Dimensional Flows About Aircraft Configurations. Computers and Fluids 1, 185, 1973.

9. Moretti, G. and Abbett, M.: A Time-Dependent Computational Method for Blunt Body Flows. AIAA J., 4, 2136, 1966.

10. Moretti, G. and Bleich, G.: Three-Dimensional Flow Around Blunt Bodies. AIAA J., 5, 1557, 1967.

11. Moretti, G. and Pandolfi, M.: Entropy Layers. Computers and Fluids, 1, 1, pp. 19-35, January 1973.

12. Moretti, G. and Pandolfi, M.: Analysis of the Inviscid Flow About a Yawed Cone. Preliminary Studies. Polytechnic Institute of Brooklyn, PIBAL Report No. 72-18, AD 745782, May 1972.

13. Nieuwland, G.Y. and Spee, B.M.: Transonic Airfoils: Recent Developments in Theory, Experiment, and Design. Annual Review of Fluid Mechanics, Vol. 5, 1973.

14. MacCormack, R.W.: The Effect of Viscosity in Hypervelocity Impact Cratering. AIAA 7th Aerospace Sciences Meeting, AIAA Paper No. 69-354, 1969.

15. Moretti, G.: Transient and Asymptotically Steady Flow of an Inviscid, Compressible Gas Past a Circular Cylinder. Polytechnic Institute of Brooklyn, PIBAL Report No. 70-20, AD 708898, April 1970.

16. Richtmyer, R.D.: Methods for (Generally Unsteady) Flows with Shocks: A Brief Survey. Presented at the 3rd International Conference on Numerical Methods in Fluid Mechanics, Paris 1972, Lecture Notes in Physics, 18; p. 72, 1973.

PIBAL MAILING LIST

P-1

Dr. R. Sedney
Exterior Ballistic Lab.
BRL-ARDC
Aberdeen Proving Ground
Maryland 21005

NASA
Attn: Dr. H.H. Kurzweg
400 Maryland Ave., SW
Washington, D.C. 20546

NASA
Langley Research Center
Attn: Dr. J.V. Becker
Chief, Aero-Physics
Hampton, Va. 23365

Chief, Bureau of Naval Weapons
Dept. of the Navy
Attn: Research Division
Washington, D.C. 20360

Engineering Societies Lib.
Attn: Acquisitions Dept.
345 East 47th St.
New York, N.Y. 10017

Int'l. Aerospace Abstract
1290 Sixth Ave.
New York, N.Y. 10019

Aerojet General Corp.
Attn: Library
P.O. Box 296
Azusa, Calif. 91703

Dr. Harris Gold
Senior Consultant Sci.
AVCO Missile Systems Div.
201 Lowell St.
Wilmington, Mass. 01887

Mr. Philip Levine, Chief
Aerodynamics Staff
AVCO Res. & Advanced Dev.
201 Lowell St.
Wilmington, Mass. 01887

Dr. Adrian Pallone
AVCO Res. & Advanced Dev.
201 Lowell St.
Wilmington, Mass. 01887

AVCO-Everett Research Lab.
Attn: Research Library
2385 Revere Beach Pkway.
Everett, Mass. 02149

AVCO Missile Systems Div.
Attn: Research Library
201 Lowell Street
Wilmington, Mass. 01887

Boeing Scientific Res. Labs.
Attn: Research Library
P.O. Box 3981
Seattle, Washington 98124

Bunker Ramo Corp.
31717 La Tienda Drive
Westlake Village, Calif. 91361

Univ. of California
Engineering & Math. Sci. Library
Serials Section
Los Angeles, Calif. 90024

Calif. Inst. of Technology
Attn: JPL Library
4800 Oak Grove Drive
Pasadena, Calif. 91102

Calif. Inst. of Technology
Guggenheim Aero. Lab.
Attn: Library (Route to Prof. Liepmann)
Pasadena, Calif. 91102

Cornell Aero. Lab., Inc.
Attn: Library
4455 Genessee Street
Buffalo, New York 14221

Cornell University
Graduate School of Aero. Engineering
Attn: Library (Route to Prof. W.R. Sears)
Ithaca, N.Y. 14850

Fairchild-Hiller
Republic Aviation Div.
Attn: Reentry Simulation Lab.
Farmingdale, N.Y. 11735

General Applied Sci. Labs.
Attn: Library
Merrick & Stewart Aves.
Westbury, N.Y. 11590

General Dynamics
Convair Aerospace Div.
Interdivision Res. Library
P.O. Box 12009
San Diego, Calif. 92112

General Electric Co.
Attn: L. Chasen, Mgr.
MSVD Library
Valley Forge Space Tech. Center
King of Prussia, Pa. 19406

Mr. Walter Daskin
General Electric Co.
Rm. 3034
3198 Chestnut St.
Philadelphia, Pa. 19101

Dr. Henry Lew
General Electric Co.
Space Sciences Lab.
Valley Forge Space Tech. Ctr
King of Prussia, Pa. 19406

Harvard University
Dept. of Applied Physics
Attn: Library (Route to Prof. H.W. Emmons)
Cambridge, Mass. 02138

Harvard University
Dept. of Engineering Sci.
Attn: Library
Cambridge, Mass. 02138

University of Illinois
Aeronautical Institute
Attn: School of Engrg.
Urbana, Ill. 61803

Illinois Inst. of Tech.
Armour Research Foundation
Attn: Library
Chicago, Ill. 60616

The Johns Hopkins Univ.
Dept. of Mechanics
Attn: Library (Route to
Profs. Klauser & Corrsin
Baltimore, Md. 21218

Marquardt Corp.
Attn: Library
Van Nuys, Calif. 91404

Research Library-6366
Martin-Marietta Corp.
P.O. Box 179
Denver, Colo. 80201

Univ. of Maryland
Inst. of Fluid Dynamics
and Applied Math.
College Park, Md. 20742

Univ. of Maryland
Attn: Engineering Library
College Park, Md. 20742

Mass. Inst. of Technology
Attn: Aeronautics Library
Cambridge, Mass. 02139

Dr. R.F. Probstein
Mass. Inst. of Technology
Dept. of Mechanical Eng.
Cambridge, Mass. 02139

Mass. Inst. of Technology
Attn: Dr. Leon Trilling
Fluid Dynamics Res. Group
Cambridge, Mass. 02139

Univ. of Michigan
Dept. of Aero. Eng.
Attn: Library
East Engineering Bldg.
Ann Arbor, Mich. 48106

Prof. Mahlon C. Smith
Dept. of Mechanical Eng.
Michigan State Univ.
East Lansing, Mich. 48823

University of Minnesota
Institute of Technology
Attn: Engineering Library
Minneapolis, Minn. 55414

North American Aviation, Inc
Attn: Mr. H.H. Crotsley
Chief, Aero. Sci.
Los Angeles Int'l. Airport
Los Angeles, Calif. 90045

Ohio State University
Dept. of Aero. Eng.
Attn: Library
Columbus, Ohio 43210

Pennsylvania State Univ.
Dept. of Aero. Eng.
Attn: Library
University Park, Pa. 16802

Princeton University
Dept. of Aero. Eng.
Attn: Library
Princeton, N.J. 08540

Princeton University
James Forrestal Res. Ctr.
Attn: Library (Route to
Prof. S. Bogdonoff)
Princeton, N.J. 08540

Dr. R. Goulard
Purdue University
School of Aero. & Eng. Sci.
Lafayette, Indiana 47907

Rensselaer Polytechnic Inst
Dept. of Aero. Eng.
Attn: Library
Troy, New York 12180

RIAS, Inc.
Attn: Library
1450 S. Rolling Road
Baltimore, Md. 21227

Southwest Research Inst.
Attn: Appl. Mechanics
Reviews
8500 Culebra Road
San Antonio, Texas 78228

Stanford University
Dept. of Aero. Eng.
Attn: Library
Stanford, Calif. 94305

Dr. Milton Van Dyke
Dept. of Aero. & Astro.
Stanford University
Stanford, Calif. 94305

Virginia Polytechnic Inst.
Carol M. Newman Library
Blacksburg, Va. 24061

George Washington Univ.
Library, Reports Section
Washington, D.C. 20006

Dr. N. Ness
Univ. of West Virginia
Dept. of Aero. Eng.
Morgantown, W. Va. 26506

Dr. Philip Mostov
6708 N. Cottonwood Ct.
Peoria, Illinois 61614

Douglas Aircraft Co.
Attn: Tech. Library,
Cl-290, 36-84
3855 Lakewood Blvd.
Long Beach, CA 90801

ONR Mailing List U-1
Contract N00014-67-A-0438-0009

Mr. Robert Moore
OSDDR&E (Strat. Weapons)
Room 3E 1082
The Pentagon
Washington, D.C. 20331

Dr. S.J. Lukasik
Def. Adv.Research Proj. Agency
1400 Wilson Blvd.
Arlington, Va. 22207

Defense Documentation Ctr
Cameron Station
Alexandria, Va. 22314 (12)

Director, Weapons System Evaluation Group
Off. of the Secy. of Def.
The Pentagon
Washington, D.C. 20305

Library of Congress
Science & Technology Div.
Washington, D.C. 20540

NASA Scientific & Tech. Information Facility
Attn: Acquisitions Branch (S-AK/DL)
P.O. Box 33
College Park, Md. 20740

Director of Research
Code RR
NASA
600 Independence Ave.,SW
Washington, D.C. 20546

NASA Langley Research Ctr
Langley Station
Attn: Library MS-185
Hampton, Virginia 23365

NASA Lewis Research Ctr.
Attn: Library MS 60-3
21000 Brookpark Rd.
Cleveland, Ohio 44135

Mr. R. Hoaglund, STO
Defense Advanced Research Projects Agency
1400 Wilson Blvd.
Arlington VA 22207

Natl. Bureau of Standards
Attn: Library
Washington, D.C. 20234

Technical Library
Bldg. 313
Ballistic Research Labs.
Aberdeen Proving Ground,MD 21005

National Science Foundation
Engineering Division
1800 G Street, NW
Washington, D.C. 20550

AFOSR-SREM
1400 Wilson Blvd.
Arlington, Va. 22209

Commander, R&T Div.
Air Force Systems Command
Attn: L.M. Hedgepeth(APIP-1
Wright-Patterson AFB, Ohio 45433

Elmer G. Johnson, Director (ARF)
Fluid Dynamics Facilities Laboratory
Aerospace Research Labs.
W-P AFB, Ohio 45433

ARL (ARN)
Bldg. 450
Wright-Patterson AFB, Ohio 45433

AFAPL (APRC)
Wright-Patterson AFB,Ohio 45433

Army Research Office
Attn: Dr. H. Robl
Box CM, Duke Station
Durham, No.Carolina 27706

Redston Sci. Info. Center
Army Missile Command
Attn: Chief, Documents Sec.
Redstone Arsenal, Ala. 35809

Chief, R & D
Office of Chief of Staff
Dept. of the Army
The Pentagon
Washington, D.C. 20310

Dr. F.D. Bennett
External Ballistics Lab.
Ballistic Research Labs.
Aberdeen Proving Ground
Maryland 21005

U.S. Army Mobility Equip. Res. & Dev. Center
Attn: Tech. Documents Ctr. Bldg. 315
Ft. Belvoir, Va. 22060

Off. of Naval Research (3)
Attn: Code 438
Dept. of the Navy
Arlington, Va. 22217

Office of Naval Research
Attn: Code 461
Dept. of the Navy
Arlington, Va. 22217

Office of Naval Research
Attn: Code 421
Dept. of the Navy
Arlington, Va. 22217

Director
Office of Naval Research
495 Symmer Street
Boston, Mass. 02210

Director
Off. of Naval Research
536 South Clark St.
Chicago, Ill. 60605

Naval Academy
Attn: Library
Annapolis, Md. 21402

Office of Naval Research
207 West 24th St.
New York, N.Y. 10011

Naval Ship Research and
Development Center
Code 5643
Bethesda, Md. 20034

Commanding Office and
Director
U.S. Naval Civil Eng. Lab.
Port Hueneme, CA 93041

Director
Off. of Naval Research
1030 East Green St.
Pasadena, Calif. 91101

Dr. Harvey R. Chaplin
Code 16
Naval Ship Research and
Development Center
Bethesda, Md. 20034

U.S. Naval Missile Center
Attn: Technical Library
Point Mugu, CA 93041

Tech. Library, Bldg. 313
Ballistic Research Labs.
Aberdeen Proving Ground
Maryland 21005

Naval Ship Research and
Development Center
Code 1800
Bethesda, Md. 20034

Mr. J. Enig
Rm. 3-252
Naval Ordnance Laboratory
White Oak
Silver Spring, Md. 20910

Office of Naval Research
San Francisco Area Office
760 Market St., Rm. 447
San Francisco, CA 94102

Miss Joanna Schot (Code 1843)
Naval Ship Research and
Development Center
Bethesda, Md. 20034

Commander
Naval Ordnance Laboratory
Attn: Dr. R.E. Wilson
Aeroballistics Div.
Silver Spring, Md. 20910

Naval Air Systems Comm.
Tech. Library Div.
(AIR-604)
Washington, D.C. 20361

Mr. F.E. West (Code 1602)
Naval Ship Research and
Development Center
Bethesda, Md. 20034

Dr. J.M. Solomon
Naval Ordnance Lab.
White Oak
Silver Spring, Md. 20910

Mr. R. Siewert (AIR-320D)
Naval Air Systems Comm.
Washington, D.C. 20361

Naval Ordnance Systems
Command
Attn: ORD 913 (Library)
Washington, D.C. 20360

Naval Ordnance Laboratory
Attn: Library
Silver Spring, Md. 20910

Director (6)
Naval Research Laboratory
Attn: Library, Code 2629
(ONRL)
Washington, D.C. 20375

Naval Ordnance Systems
Command
Attn: ORD 035
Washington, D.C. 20360

Technical Library
Naval Ordnance Station
Indian Head, Md. 20640

Director (6)
Naval Research Laboratory
Attn: Code 2627
Washington, D.C. 20375

Mr. W. Koven (AIR 320)
Naval Air Systems Command
Washington, D.C. 20361

Commanding Officer
Naval Ordnance Station
Louisville, Ky. 40214

Mr. R. Feldhuhn
Code 313
Naval Ordnance Lab.
Silver Spring, MD 20910

Dr. T.D. Taylor
Fluid Mechanics Dept.
The Aerospace Corp.
P.O. Box 92957
Los Angeles, CA 90009

AVCO Corp.
Attn: Research Library
201 Lowell St.
Wilmington, Mass. 01887

Engineering Division
Calif. Inst. of Technology
Pasadena, CA 91109

Naval Weapons Center
Code 753
China Lake, CA 93555

Chief of Aerodynamics
Missile Systems Div.
AVCO Corp.
201 Lowell St.
Wilmington, Mass. 01887

Prof. H. Liepmann
Dept. of Aeronautics
Calif. Inst. of Technology
Pasadena, CA 91109

Naval Postgraduate School
Attn: Tech. Repts. Lib.
Monterey, CA 93940

Prof. J.T.C. Liu
Div. of Engineering
Brown University
Providence, Rhode Is.
02912

Prof. L. Lees
Guggenheim Aero. Lab.
Calif. Inst. of Technology
Pasadena, CA 91109

Dr. Barry L. Clark
Code GB
Naval Weapons Lab.
Dahlgren, VA 22418

AVCO-Everett Research Lab.
Attn: B. Spence, Tech.Lib.
2385 Revere Beach Parkway
Everett, Mass. 02149

Dr. S.A. Berger
Dept. of Mech. Eng.
Univ. of California
Berkeley, CA 94720

Technical Library
Naval Weapons Lab.
Dahlgren, Va. 22418

Battelle-Defender Info.
Analysis Center
Battelle Memorial Inst.
505 King Ave.
Columbus, Ohio 43201

Prof. M. Holt
Div. of Aero. Sciences
University of California
Berkeley, CA 94720

Engrg. Societies Library
345 E. 47th St.
New York, N.Y. 10017

Bell Telephone Labs.,Inc.
Technical Reports Center
Whippany Laboratory
Whippany, N.J. 07981

Prof. A.K. Oppenheim
Div. of Mechanical Eng.
University of California
Berkeley, CA 94720

Aerojet-General Corp.
Attn: Library
P.O. Box 296
Azusa, CA 91702

Prof. J.H. Clarke
Brown University
Div. of Engineering
Providence, R.I. 02912

Dr. L. Talbot
Dept. of Engineering
University of California
Berkeley, CA 94720

Prof. R.G. Stoner
Dept. of Physics
Arizona State University
Tempe, Arizona 85721

Prof. P.S. Maeder
Brown University
Div. of Engineering
Providence, R.I. 02912

Prof. A.J. Chorin
Dept. of Mathematics
Univ. of California
Berkeley, CA 94720

Dr. Antonio Ferri
Advanced Technology Labs.
Merrick & Stewart Aves.
Westbury, NY 11590

Prof. L. Sirovich
Div. of Applied Math.
Brown University
Providence, R.I. 02912

Univ. of So. California
Engineering Library
Box 77929
Los Angeles, CA 90007

Dr. J. Trulio
Applied Theory, Inc.
1010 Westwood Blvd.
Los Angeles, CA 90024

Dr. Gordon Hall
Dept. of Mechanical Eng.
State Univ. of New York
at Buffalo
Buffalo, N.Y. 14214

Dr. H.K. Cheng
Dept. of Aero. Eng.
Univ. of So. California
University Park
Los Angeles, CA 90007

Dr. H. Yoshihara
Mail Zone 630-00
General Dynamics-CONVAIR
P.O. Box 1128
San Diego, CA 92112

Dr. S.M. Yen
Coordinated Science Lab.
University of Illinois
Urbana, Ill. 61801

Prof. James C. Wu
School of Aerospace Eng.
Georgia Inst. of Technology
Atlanta, GA 30332

School for Applied Math.
Indiana University
Bloomington, Indiana
47401

Prof. S. Weinbaum
Dept. of Mech. Eng.
City Univ. of New York
New York, NY 10031

General Dynamics
Convair Aerospace Div.
Interdivision Res. Library
P.O. Box 12009
San Diego, CA 92112

Jet Propulsion Lab.
Attn: Library
4800 Oak Grove Drive
Pasadena, CA 91103

Prof. R.T. Davis
Dept. of Aero. Eng. and
Appl. Mech.
University of Cincinnati
Cincinnati, Ohio 45221

Mr. L.I. Chasen, Manager
MSVD Library
General Electric Co.
P.O. Box 8555
Philadelphia, Pa. 19104

Lockheed Missiles & Space
Tech. Information Center
3251 Hanover St.
Palo Alto, CA 91301

Mr. R.J. Vidal
Calspan Corp.
P.O. Box 235
Buffalo, N.Y. 14221

Dr. H.T. Nagamatsu
General Electric Co.
Research Laboratory
P.O. Box 8
Schenectady, N.Y. 12301

LTV Aerospace Corp.
Tech. Library 2-51131
P.O. Box 5907
Dallas, Texas 75222

Dr. J. Erickson
Calspan Corp.
P.O. Box 235
Buffalo, NY 14221

Dr. B. Grossman
Grumman Aerospace Corp.
Propulsion Lab.
Plant 35, Dept. 423
Bethpage, NY 11714

Prof. S.F. Shen
Graduate School of Aero.
Engineering
Cornell University
Ithaca, NY 14850

Dr. Frank Lane
KLD Associates, Inc.
7 High Street
Huntington, NY 11743

Prof. E.L. Resler, Jr.
Cornell University
Graduate School of Aero.
Engineering
Ithaca, N.Y. 14850

Dr. Roger P. Heinisch
Honeywell, Inc.
Systems & Research Div.
2345 Walnut St.
St. Paul, Minn. 55113

Prof. W.R. Sears
Cornell University
Graduate School of Aero.
Engineering
Ithaca, N.Y. 14850

Prof. H.S. Stillwell
Dept. of Aero. & Astro.Eng.
University of Illinois
Urbana, Ill. 61803

Prof. R.F. Probstein
Dept. of Mechanical Eng.
Mass. Inst. of Technology
Cambridge, Mass. 02139

Prof. A.H. Shapiro
Dept. of Mechanical Eng.
Mass. Inst. of Technology
Cambridge, Mass. 02139

McDonnell Aircraft Corp.
Attn: Engineering Lib.
Dept. 218,
Bldg. 101
P.O. Box 516
St. Louis, Mo. 63166

Dr. R.J. Hakkinen
Mgr.-Research, Flight Sci
McDonnell Douglas Res. Labs.
Dept. 222,Bldg.33,Rm.458
P.O. Box 516
St. Louis, Mo. 63166

Mr. Richard Coleman
Mechanical Technology,Inc
968 Albany-Shaker Road
Latham, N.Y. 12110

Midwest Research Inst.
425 Volker Blvd.
Attn: Library
Kansas City, Mo. 64110

Prof. E.R.G. Eckert
Univ. of Minnesota
241 Mechanical Eng.Bldg.
Minneapolis,Minn.55455

Dr. R. Vaglio-Laurin
New York University
Dept. of Aeronautics
New York, N.Y. 10453

North American Aviation,Inc
Space & Info. Systems Div.
12214 Lakewood Blvd.
Downey, Calif. 90240

Dr. B.H. Pridmore Brown
Northrop Corp.
Norair Div.
1001 E. Broadway
Hawthorne, CA 90250

Prof. O. Burggraf
Dept. of Aero. & Astro.Eng.
Ohio State University
Columbus, Ohio 43220

Prof. Ting Yi Li
Dept. of Aero. & Astro. Eng.
Ohio State University
2036 Neil Ave.
Columbus, Ohio 43210

Prof. S. Bogdonoff
Gas Dynamics Laboratory
Princeton University
Princeton, N.J. 08540

Prof. S.I. Cheng
Gas Dynamics Laboratory
Forrestal Campus
Princeton University
Princeton, N.J. 08540

Dr. R. Goulard, Director
Project SQUID
Thermal Sci. & Propulsion Center
Purdue University
West Lafayette, IN 47907

Radio Corp. of America
Attn: Mrs. E.K. Daly
Eng. Lib. 127-223
Moorestown, N.J. 08057

Library
The Rand Corp.
1700 Main St.
Santa Monica, CA 90401

Prof. A. Chapman,Chairman
Mechanical Eng. Dept.
William M. Rice Inst.
Box 1892
Houston, Texas 77001

Prof. M. Lessen, Head
Dept. of Mechanical Eng.
University of Rochester
River Campus Station
Rochester, N.Y. 14627

Mr. C.C. Hudson
Sandia Corp.
Sandia Base
Albuquerque, N.M. 87115

Editor
Applied Mechanics Review
Southwest Research Inst.
8500 Culebra Rd.
San Antonio, Texas 78206

Dr. C. Cook
Stanford Research Inst.
Menlo Park, CA 94025

Prof. M. Van Dyke
Dept. of Aero. Eng.
Stanford University
Stanford, CA 94305

Prof. W.G. Vincenti
Dept. of Aero. & Astro.
Stanford University
Stanford, CA 94305

Prof. K. Karamcheti
Dept. of Aero. Eng.
Stanford University
Stanford, CA 94305

Prof. A.H. Nayfeh
Dept. of Eng. Mech.
Virginia Polytechnic Inst. and State Univ.
Blacksburg, VA 24061

Supervisor, Tech. Lib. Sec.
Thiokol Chemical Corp.
Wasatch Division
Brigham City, Utah 84302

Dr. P.K. Dai
R1/2178
TRW Systems
One Space Park
Redondo Beach, CA 90278

Dr. G.A. Inger
Dept. of Aero. Eng.
Virginia Polytechnic Inst. and State University
Blacksburg, VA 24061

United Aircraft Corp.
Attn: Library
Silver Lane
East Hartford, Conn. 06103

Department Librarian
Univ. of Washington
Dept. of Aero. Eng.
Seattle, Wash. 98105

Dr. Eric Baum
TRW Systems Group, Inc.
One Space Park
Redondo Beach, CA 90278

Dr. A. Hertzberg
Director of Aero. Lab.
University of Washington
Seattle, Wash. 98105

United Aircraft Corp.
Research Laboratory
Attn: Dr. W.R. Briley
East Hartford, Conn. 06108

Prof. P.P. Wegener
Dept. of Eng. & Appl. Sci.
Yale University
New Haven, Conn. 06520

McGill University
Supersonic-Gasdynamics Research Lab.
Room 363
Montreal 2, CANADA

National Research Council
Attn: Miss O.M. Leach
Librarian
Montreal Road
Ottawa 7, CANADA

Prof. I.I. Glass
University of Toronto
Inst. for Aero. Studies
Toronto 181, CANADA

The Library
University of Toronto
Inst. for Aero. Studies
Toronto 181, CANADA

Dr. N.C. Freeman
Aeronautics Dept.
Imperial College
London S.W. 7, ENGLAND

Dr. L.F. Crabtree
Royal Aircraft Establish.
Ministry of Aviation
Aerodynamics Dept.
Farnborough, Hants, ENGLAND